ANOMALOUS ELECTRIC DIPOLE INTERNAL CONVERSION

Thesis by

Ralph Stuart Hager

In Partial Fulfillment of the Requirements

For the Degree of

Doctor of Philosophy

California Institute of Technology

Pasadena, California

1966

(Submitted March 9, 1966)

ACKNOWLEDGMENTS

Many people have contributed to the success of these experiments. The author wishes to thank: Professor F. Boehm, for his interest and support; Dr. E. Kankeleit for his assistance in the completion of this thesis; Dr. E. Seltzer for many important contributions in all phases of this work; Dr. P. Alexander, Professor Emeritus J.W.M. DuMond, and Mr. H. Henrikson for the design and construction of the $\sqrt{2}$ π spectrometer; the California Institute of Technology, the Atomic Energy Commission, and the National Science Foundation for financial assistance; and, my wife, Mary, for her encouragement and forbearance.

ABSTRACT

Electric dipole internal conversion has been experimentally studied for several nuclei in the rare earth region. Anomalies in the conversion process have been interpreted in terms of nuclear structure effects. It was found that all the experimental results could be interpreted in terms of the $j \cdot r$ type of penetration matrix element; the $j \cdot \nabla$ type of penetration matrix element was not important. The ratio λ of the E1 $j \cdot r$ penetration matrix element to the E1 gamma-ray matrix element was determined from the experiments to be:

Lu^{175},	396 keV,	$\lambda = -1000 \pm 100$;
	282 keV,	$\lambda = 500 \pm 100$;
	144 keV,	$\lambda = 500 \pm 250$;
Hf^{177},	321 keV,	$\lambda = -1400 \pm 200$;
	208 keV,	$\lambda = -90 \pm 40$;
	72 keV,	$\lvert\lambda\rvert \leq 650$;
Gd^{155},	86 keV,	$\lambda = -150 \pm 100$;
Tm^{169},	63 keV,	$\lambda = -100 \pm 100$;
W^{182},	152 keV,	$\lambda = -160 \pm 80$;
	67 keV,	$\lambda = -100 \pm 100$.

Predictions for λ are made using the unified nuclear model.

TABLE OF CONTENTS

LIST OF TABLES

LIST OF FIGURES

CHAPTER I

INTRODUCTION

The de-excitation of a nucleus from an excited state can proceed by emission of a gamma-ray or by directly transferring the excitation energy to one of the atomic electrons surrounding the nucleus. This latter process is referred to as internal conversion and competes with the process of gamma-ray emission. The internal conversion electron will be ejected from the atom with kinetic energy equal to the available excitation energy minus the binding energy of the electron in the atom. Conversion of the electron occurs through the interaction of the electron with the nuclear currents and charges via the electromagnetic field. The ratio of the rate of electron ejection N_e to the rate of gamma-ray emission N_γ is the internal conversion coefficient

$$\alpha = N_e/N_\gamma. \qquad (1)$$

For a given transition the conversion can take place in any atomic subshell which allows for energy conservation and so we have partial conversion coefficients α_K, α_{L_I}, etc.

Conversion coefficients are strongly dependent on the transition energy, the atomic number, and multipolarity of the transition. Calculation and tabulation of conversion coefficients as a function of these quantities have been carried out by Rose[1] and by Sliv and Band[2]. Comparison of these theoretical coefficients with experimental measurements of absolute coefficients or relative coefficients (K/L_I, L_I/L_{II}, etc.) is very useful for determination of

transition multipolarities thereby giving information concerning spin and parity differences in nuclear level schemes.

When the nucleus is treated as a point charge the conversion coefficients are independent of nuclear structure since the same nuclear matrix elements occur in both N_e and N_γ and therefore cancel. When the finite size of the nucleus is taken into account the conversion coefficient has the form

$$\alpha = \sum_f \alpha_f |1 + C_f \lambda|^2 \qquad (2)$$

where the sum is over final electron states. α_f is the partial conversion coefficient calculated with electron wave functions in the field of a nucleus with finite size. This influence of the finite size on the conversion coefficients is referred to as a static nuclear effect. α_f depends on nuclear structure only through the assumption of the nuclear charge density. Sliv and Band[2] have shown this dependence to be very weak for a reasonable choice of the charge density. The importance of this static effect of the nuclear charge size was pointed out by Sliv[3].

The term $C_f\lambda$, which is usually small in comparison with one, represents the contribution to the conversion coefficient when the atomic electron is converted inside the nucleus. In actuality, there are many terms in $C_f\lambda$ of Eq. (2) but for the moment we will consider only one such term, assuming all the others can be neglected. C_f like α_f depends only on the electron wave functions and is usually small since it is determined by the size of the electron wave function in the region of the nucleus. The quantity λ is a ratio of nuclear matrix elements

(or more precisely, the ratio of the penetration matrix element to the normal gamma-ray matrix element). If λ has its dimensional value then $C_f\lambda$ will make only a few percent correction at most to α_f. Such terms are called penetration terms and they are the result of dynamic nuclear effects. Since the nuclear matrix elements no longer cancel, a nuclear model is required for a theoretical estimate of λ. Church and Weneser[4] were first to point out the importance of dynamic effects in internal conversion.

The static effects can be quite significant, sometimes as large as 50%, and have been taken into account in the calculations by Rose and by Sliv. The dynamic effects are less than a few percent except in some cases where the gamma-ray transition is hindered. In these exceptions the penetration contribution can be rather large and the internal conversion process will appear anomalous. Such anomalies in the conversion process have been observed by several workers[5-12] but not always analyzed in terms of nuclear theory. It should be emphasized that for each final electron state the static and dynamic contributions add coherently so the phases as well as the magnitude of these quantities must be known to properly extract the nuclear information.

This thesis deals with the observation and study of penetration effects in E1 internal conversion. The nuclear structure parameters λ are determined for several hindered gamma-ray transitions for nuclei in the rare earth region. These are determined experimentally by observing anomalies in the conversion process. The determination of λ means the penetration matrix element is known since the gamma-ray matrix element can be determined rather well from other experiments.

These penetration matrix elements involve different operators and therefore provide new types of nuclear information. The determination of nuclear matrix elements when compared with the predictions of a nuclear model can provide a test or determine limitations of the nuclear model.

CHAPTER II

GENERAL CONSIDERATION OF THE PENETRATION CONTRIBUTIONS TO E1 INTERNAL CONVERSION

Form of the Penetration Matrix Elements

If $M_{fi}(EL)$ is the matrix element of the retarded electromagnetic interaction between the nuclear transition currents and those of the converting electron, then the rate for emission of electrons from initial state i is proportional to $\sum_f |M_{fi}(EL)|^2$ where the summation is over all final electron states. The EL is written explicitly to point out that we wish to consider only electric multipoles. M_{fi} can be written in the following way to exhibit its dependence on the normal conversion and penetration terms*):

$$M_{fi}(EL) = N_{LM}\left[R_{fi}q_L\int d\tau_n \vec{j}_n\cdot\vec{A}^*_{LM}(kr_n) + \int d\tau_n \vec{j}_n\cdot\vec{\nabla}\,\Phi_{fi}(r_n)\; Y^*_{LM}(\hat{r}_n) + \int d\tau_n \vec{j}_n\cdot\frac{\hat{r}_n}{r_n}\,\Theta_{fi}(r_n)\; Y^*_{LM}(\hat{r}_n)\right] . \qquad (3)$$

N_{LM} represents the result of integration over the electron angular coordinates and R_{fi}, $\Phi_{fi}(r_n)$, and $\Theta_{fi}(r_n)$ are obtained from integrals over the electron radial coordinate. The exact form of the functions R_{fi}, Φ_{fi}, and Θ_{fi} are given in Appendix I along with an abbreviated derivation of the penetration terms. Kramer[13], Kramer and Nilsson[14], and Green and Rose[15] give a complete derivation of the separation of

---

*) The units used in this paper are $\hbar = c = 1$. Lengths and times will therefore have units of reciprocal energy. In these units $e^2 = \alpha \approx 1/137$.

M_{fi} into normal and penetration terms. Y_{LM} are the spherical harmonics, A_{LM} are the vector spherical harmonics, and j_n is the nuclear current. The factor q_L is introduced for convenience in defining the functions Θ and Φ and is just a constant given by

$$q_L = k\sqrt{\frac{L}{L+1}}\ \frac{(2L+1)!!}{(kR)^L} \quad .$$

R is the nuclear radius and k is the transition energy. The first term in Eq. (3) represents the usual conversion contribution and the last two terms are the penetration contributions. The factor $\int d\tau_n \vec{j}_n \cdot \vec{A}^*_{LM}$ is the usual matrix element for gamma-ray emission.

At the present time it suffices to know that the penetration weighting functions will be used in the form of a power series in the variable r_n/R. The form of these functions for E1 conversion are:

$$\Phi_{fi}(r_n) = \gamma_1\left(\frac{r_n}{R}\right)^3 + \gamma_2\left(\frac{r_n}{R}\right)^5 + \cdots \ ,$$

$$\Theta_{fi}(r_n) = \beta_1\left(\frac{r_n}{R}\right)^3 + \beta_2\left(\frac{r_n}{R}\right)^5 + \cdots . \qquad (4)$$

All the dependence of the penetration contributions on the atomic electrons is contained in the constants γ_j and β_j. These constants exhibit a specific dependence on the electron initial and final states and their form will be determined later since they are required for analysis of the experiments.

Dropping the subscript n we can write the penetration terms for E1 conversion as

$$\sum_{m=1}^{\infty}\left[\gamma_m\int d\tau\ \vec{j}\cdot\vec{\nabla}\, r^{2m+1}\, Y^*_{1M}(\hat{r}) + \beta_m\int d\tau\ \vec{j}\cdot\hat{r}\, r^{2m}\, Y^*_{1M}(\hat{r})\right]\frac{1}{R^{2m+1}} \cdot \qquad (5)$$

With the use of the continuity equation $\vec{\nabla}\cdot\vec{j} = ik\rho$, the first of these integrals can be put in the form

$$\int d\tau\ \vec{j}\cdot\vec{\nabla}\ r^{2m+1}\ Y^*_{1M}(\hat{r}) = -\ ike\int d\tau\ \psi^*_f\ r^{2m+1}Y^*_{1M}(\hat{r})\ \psi_i\ . \qquad (6)$$

The second term in (5) cannot be reduced without invoking a specific form of the nuclear current. Let us assume the nuclear current to be of the form $\vec{j} = \vec{j}_c + \vec{j}_s$ where $\vec{j}_c$ is the convection current

$$\vec{j}_c = \frac{e}{2iM}\left[\psi^*_f\vec{\nabla}\psi_i - (\vec{\nabla}\psi_f)^*\psi_i\right] \qquad (7)$$

and j_s is the spin current

$$\vec{j}_s = \frac{e\mu}{2M}\vec{\nabla}\times\psi^*_f\vec{\sigma}\psi_i\ . \qquad (8)$$

M and μ are the nucleon mass and the magnetic moment; ψ_f and ψ_i are the final and initial nuclear wave functions. The components of the vector $\vec{\sigma}$ are the usual Pauli spin matrices. We can then write the penetration contribution from the convection current in the form (see Appendix II)

$$\int d\tau\ \vec{j}_c\cdot\hat{r}\ r^{2m}\ Y^*_{1M} = \frac{e}{iM}\int d\tau\ \psi^*_f\ r^{2m-1}\ Y^*_{1M}(\vec{r}\cdot\vec{\nabla} + n + 1)\psi_i\ . \qquad (9)$$

The contribution from the spin current has the form

$$\int d\tau\ \vec{j}_s\cdot\hat{r}\ r^{2m}Y^*_{1M} = \frac{e\mu}{2Mi}\int\psi^*_f\ \vec{\sigma}\cdot(\vec{L}\ r^{2m-1}Y^*_{1M})\psi_i d\tau\ . \qquad (10)$$

The gamma-ray matrix element $\int d\tau\ \vec{j}\cdot\vec{A}^*_{1M}$ in the long wavelength limit gives the familiar E1 matrix element (see Appendix II)

$$\int d\tau\ \vec{j}\cdot\vec{A}^*_{1M} = \frac{1}{q_1}\int d\tau\ \psi^*_f\ r\ Y^*_{1M}\ \psi_i\ . \qquad (11)$$

The operators for these four types of matrix elements are shown in Table I. The lowest order penetration operators are obtained by setting m = 1.

Table I

Gamma-Ray and Penetration Operators for E1 Conversion

Type of Matrix Element	General Term in Expansion	Lowest Order Term in Expansion
Gamma-ray	$r\ Y^*_{1M}$	$r\ Y^*_{1M}$
Penetration $(j\cdot\nabla)$	$r^{2m+1}\ Y^*_{1M}$	$r^3 Y^*_{1M}$
Penetration $(j_c\cdot r)$	$r^{2m-1}\ Y^*_{1M}\ (\vec{r}\cdot\vec{\nabla} + n + 1)$	$r\ Y^*_{1M}(\vec{r}\cdot\vec{\nabla} + 2)$
Penetration $(j_s\cdot r)$	$\vec{\sigma}\cdot\ (\vec{L} r^{2m-1}\ Y^*_{1M})$	$\vec{\sigma}\cdot\ (\vec{L}\ r\ Y^*_{1M})$

Form of the Nuclear Structure Parameters $\lambda(j\cdot r)$ and $\lambda(j\cdot\nabla)$

Using Eq. (3) the conversion coefficient can be written in the form

$$\alpha_i = \sum_f \text{const.} \left| R_{fi} + \frac{\int \vec{j}\cdot\vec{\nabla}\ \Phi_{fi}(r)\ Y^*_{1M}(\hat{r})}{q_1 \int \vec{j}\cdot\vec{A}^*_{1M}} + \frac{\int \vec{j}\cdot\frac{\hat{r}}{r}\ \Theta_{fi}(r)\ Y^*_{1M}(\hat{r})}{q_1 \int \vec{j}\cdot\vec{A}^*_{1M}} \right|^2 \tag{12}$$

which we write as

$$\alpha_i = \sum_f \text{const} \left| R_{fi} + \sum_{m=1}^{\infty} (\gamma_m \lambda_m\ (j\cdot\nabla) + \beta_m \lambda_m (j\cdot r)) \right|^2 . \tag{13}$$

In this equation γ_m and β_m are the same constants that appear in Eq. (4). $\lambda_m(j\cdot\nabla)$ and $\lambda_m(j\cdot r)$ are given by

$$\lambda_m(j\cdot\nabla) = \frac{\int \vec{j}\cdot\vec{\nabla}\left(\frac{r}{R}\right)^{2m+1} Y^*_{1M}}{\int \vec{j}\cdot\vec{\nabla}\left(\frac{r}{R}\right) Y^*_{1M}} \quad ,$$

$$\lambda_m(j\cdot r) = \frac{\int \vec{j}\cdot\frac{\hat{r}}{R}\left(\frac{r}{R}\right)^{2m} Y^*_{1M}}{\int \vec{j}\cdot\vec{\nabla}\left(\frac{r}{R}\right) Y^*_{1M}} \quad . \tag{14}$$

Written out in terms of the usual reduced matrix elements and the dimensionless variable $x = \sqrt{M\omega}\, r$, these parameters are

$$\lambda_m(j\cdot\nabla) = \left(\frac{1}{M\omega R^2}\right)^m \frac{\langle f||x^{2m+1}\, Y^*_1||i\rangle}{\langle f||x\, Y^*_1||i\rangle} \quad ,$$

$$\lambda_m(j\cdot r) = \frac{\omega}{k}\left(\frac{1}{M\omega R^2}\right)^m \left[\frac{\langle f||x^{2m-1}\, Y^*_1\, (\vec{x}\cdot\vec{\nabla} + m + 1)||i\rangle}{\langle f||x\, Y^*_1\,||i\rangle} + \right. \tag{15}$$

$$\left. + \frac{\frac{\mu}{2}\langle f||x^{2m-1}\,\vec{\sigma}\cdot(\vec{L}Y^*_1)||i\rangle}{\langle f||x\, Y^*_1\,||i\rangle}\right] ,$$

where ω is the oscillator shell spacing energy. We might therefore expect as a dimensional estimate*)

---

*) This is only a crude estimate since the matrix elements will many times differ by an order of magnitude.

$$\left|\frac{\lambda_m(j\cdot r)}{\lambda_m(j\cdot\nabla)}\right| \approx \frac{\omega}{k} \approx 20 - 100. \tag{16}$$

A dimensional estimate of $\frac{\beta_m}{\gamma_m}$ gives

$$\left|\frac{\beta_m}{\gamma_m}\right| \approx kR \approx (2 - 10) \times 10^{-3}. \tag{17}$$

These two estimates together indicate that the $j\cdot\nabla$ penetration contribution is the larger of the two, which, among other things, led Nilsson and Rasmussen[16] to neglect the $j\cdot r$ penetration terms in an early discussion of the subject. However, the estimates are incorrect since cancellation occurs for some of the γ_m. Consequently, as pointed out by Church and Weneser[17], it is the $j\cdot r$ penetration terms which contribute most strongly to the conversion process.

The cancellation in γ_m occurs for those electron transitions for which the total angular momentum of the initial and final electron states is 1/2, which are just the electron transitions that are expected to contribute most strongly to the penetration terms. These $1/2 \rightarrow 1/2$ transitions occur for conversion in the L_I and L_{II} subshells but not in the L_{III} subshell. Because of the cancellation the penetration contributions from the $1/2 \rightarrow 1/2$ transitions will be comparable with contributions from other transitions, e.g., $3/2 \rightarrow 1/2$ which does occur in the L_{III} subshell. It is therefore expected that $\lambda(j\cdot\nabla)$ will cause comparable anomalies in all three subshells. Conversely, since there is no cancellation in the β_m, $\lambda(j\cdot r)$ will be largest for the $1/2 \rightarrow 1/2$ transitions in the L_I and L_{II} subshells.

In previous measurements[5,11] and also in the measurements reported here all L subshell anomalies are observed only in the L_I and L_{II} subshells. L_{III} conversion is never anomalous. This trend can only be explained by a general dominance of the j·r type penetration terms.

Under normal conditions (little or no retardation of the gamma-ray transition probability) the penetration terms will make only a small correction to the normal conversion contribution. Sliv and Band in their tabulation of conversion coefficients[2] have included estimates of these terms by using a surface current model of the nucleus. In such a model the current is assumed to be of the form

$$\vec{j} = \vec{J}\,(\theta,\phi)\;\delta(r - R). \tag{18}$$

In this model $\vec{j}\cdot\hat{r} = 0$ and thus $\lambda(j\cdot r) = 0$. Using Eq. (14) and this form of the current we have

$$\lambda_m(j\cdot\nabla) = \frac{\int \vec{J}\cdot\nabla_\theta\, Y^*_{1M}}{\int \vec{J}\cdot\nabla_\theta\, Y^*_{1M}} = 1.$$

The estimate for $\lambda(j\cdot\nabla)$ is good but the estimate for $\lambda(j\cdot r)$ is unrealistic. Although under normal conditions the estimate in (16) is perhaps too large, we might expect $\lambda(j\cdot r) = 5 - 20$. Using these estimates the penetration terms contribute a correction of only a few percent to the conversion coefficient.

In this thesis we are interested in observing the effects of these penetration terms. It is clear we must have $\lambda \gg 1$ if we are going to observe anomalies in the conversion coefficients. Therefore, we will be interested only in hindered or retarded transitions hoping that the penetration contributions will not likewise be hindered.

This means that the lifetime of the nuclear state from which the transition originates must be long in comparison with some dimensional estimate of the lifetime, e.g., long compared with the Weisskopf estimate[18]. Therefore, it is possible to estimate the retardation of the gamma-ray transition for those cases where experimental lifetimes have been determined.

Selection Rules for the Unified Nuclear Model

Whether a matrix element is allowed or forbidden can be determined by consideration of the selection rules. For nuclei in the rare earth region the deformed coupling scheme is well established. Excellent reviews of the unified model have been written by Nathan and Nilsson[19] Kerman[20], and Elliot[21].

In this region far from closed shells the nucleus acquires a permanent deformation. It is then possible to approximately describe nuclear states as having collective properties and intrinsic properties. The intrinsic properties are the result of nucleonic motion in a stationary deformed nuclear field while the collective properties are the result of the slower rotational and vibrational motion of the deformed nucleus as a whole. For axially symmetric nuclei, neglecting the vibrational motion, the wave function can be written in the form

$$\psi = \text{const.} \left[D^{I}_{MK} \chi_{K} + (-1)^{I-J} D^{I}_{M-K} \chi_{-K} \right]. \qquad (19)$$

D^{I}_{MK} are the usual rotation matrices describing the rotational motion which is characterized by the quantum numbers I, M, and K, i.e., the

total (rotational + intrinsic) angular momentum, its projection on the space fixed axis, and its projection on the intrinsic nuclear axis. χ represents the intrinsic motion and J is the total intrinsic angular motion. This description rather accurately accounts for the rotational spectra observed in deformed nuclei. The low-lying levels of odd A nuclei can be understood in terms of a single particle intrinsic wave function.

Nilsson[22] has obtained solutions for the intrinsic wave functions χ by using a single particle deformed shell model Hamiltonian of the form

$$H = -\frac{1}{2M}\nabla^2 + \frac{M}{2}(\omega_\perp^2 r_\perp^2 + \omega_z^2 z^2) + C\,\vec{\ell}\cdot\vec{s} + D\,\vec{\ell}\cdot\vec{\ell}. \qquad (20)$$

In the limit of large nuclear deformations ($\omega_z \ll \omega_\perp$) the intrinsic wave functions can be characterized by the asymptotic quantum numbers[22,23]. These are the principal oscillator quantum number N, the number of oscillator quanta along the z axis (symmetry axis) n, the projection of the intrinsic orbital momentum on the z axis Λ, and the projection of the intrinsic spin on the z axis Σ. Since the rotational angular momentum has no component along the symmetry axis $K = \Lambda + \Sigma$. For realistic nuclear deformations n is not a good quantum number but there is one component of the wave function (corresponding to a particular n) which dominates the wave function. This explains the usefulness of the asymptotic quantum numbers.

The selection rules for the gamma-ray and penetration operators in Table I can be investigated in terms of the asymptotic selection rules. The selection rules for these operators have been

tabulated by Church and Weneser[24]. In practice, one generally does not have to refer to the tabulated selection rules if one is familiar with some simple rules, such as z changes only N and n, $r_{\pm} = x \pm iy$ changes only N and Λ, σ changes only Σ, etc.

Since the gamma-ray and penetration operators vary in complexity it is more likely that the penetration matrix elements will be allowed when the gamma-ray matrix element is forbidden, e.g., transitions that involve spin flip fulfill this condition. Spin flip occurs in many of the cases investigated in this work. For example, for M = - 1 the gamma-ray and spin current penetration (m = 1) operators are proportional to r_- and $(z\sigma_- - r_-\sigma_z)$. If the asymptotic initial and final states are $|Nn\Lambda+\rangle$ and $|N - 1, n - 1, \Lambda - 1\rangle$, then r_- and $r_-\sigma_z$ are forbidden whereas $z\sigma_-$ is allowed.

The asymptotic classification will be presented in the next chapter for all the transitions investigated in this work.

Still another selection rule, which is the result of the collective properties of these deformed nuclei, is the K selection rule[19]. This selection rule refers to transitions between rotational bands (interband transitions) with different K values. Applied specifically to the case of E1 transitions this rule states that transitions between two rotational bands for which $|\Delta K| \geq 2$ are forbidden. Since K forbiddenness is a consequence of the collective nuclear properties it applies both to the gamma-ray and to the penetration matrix elements. Therefore, K forbidden transitions certainly offer no advantage over K allowed transitions unless it is known that the transition is interesting for some other reason.

CHAPTER III

CASES SELECTED FOR INVESTIGATION

Consideration of the selection rules can be used as a rough guide in selecting cases for which an observable anomaly might be expected. After an interesting case has been found, consideration must be given to the experimental feasibility. Special attention should be given to the following:

1. Halflife for decay of the parent isotope
2. Specific activity and availability of the source material
3. Strength of the transition under investigation, and
4. Methods for source preparation.

To a great extent the success of the experiments depends on how well the experiments can be done. Extreme difficulty in any of these areas would probably make the experiment very hard to carry out.

With all of these considerations in mind the cases presented in Table II were selected for study. Each of these cases will be discussed in detail in Chapter VI. At the present time we make only a few remarks concerning these cases.

TABLE II

E1 TRANSITIONS SELECTED FOR INVESTIGATION

Nucleus	γ-Ray Energy (keV)	State Assignments $I\pi K\,[Nn\Lambda]$		$T_{\frac{1}{2}}$ (exp) (sec) f)	$T_{\frac{1}{2}}$ (part) (sec) f,g)	Retardation Factor i)	Asymptotic Classification j)			
		Initial	Final				γ-Ray	Penetration (n=1) $\langle j_c \cdot r \rangle$	$\langle j_s \cdot r \rangle$	$\langle j \cdot \nabla \rangle$
Hf^{177} a)	321.4	$\frac{9}{2} + \frac{9}{2}\,[624]$	$\frac{7}{2} - \frac{7}{2}\,[514]$	6.3(-10)	3.5(-8)	5.4(6)	h	h	a	h
	208.4		$\frac{9}{2} -$		7.0(-10)	3.0(4)				
	71.6		$\frac{11}{2} -$		5.0(-8)	8.5(4)				
Lu^{175} b)	396.1	$\frac{9}{2} - \frac{9}{2}\,[514]$	$\frac{7}{2} + \frac{7}{2}\,[404]$	3.4(-9)	5.8(-9)	1.7(6)	h	h	a	h
	282.6		$\frac{9}{2} +$		1.1(-10)	1.2(6)				
	144.8		$\frac{11}{2} +$		9.9(-9)	1.4(6)				
Tm^{169} c)	63.1	$\frac{7}{2} - \frac{7}{2}\,[523]$	$\frac{7}{2} + \frac{7}{2}\,[404]$	3.6(-8)	7.5(-8)	8.5(4)	h	h	h k)	h
Gd^{155} d)	86.5	$\frac{3}{2} + \frac{3}{2}\,[651]$	$\frac{3}{2} + \frac{3}{2}\,[521]$	5.0(-9)	7.4(-9)	2.0(4)	h	h k)	h	h k)
W^{182} e)	152.4	3 - 2 m)	2 + 2	2.3(-9)	1.0(-8)	1.6(5)		m)		
	67.7	2 -		1.0(-9)	1.9(-9)	2.7(3)				

FOOTNOTES TO TABLE II

a) Data from Refs. 25 and 26.

b) Data from Refs. 25 and 27.

c) Data from Ref. 28.

d) Data from Refs. 27 and 29.

e) Data from Refs. 27 and 30.

f) The number in parentheses is the power of ten that multiplies the entry.

g) $T_{\frac{1}{2}}$ (part) is the partial halflife for the gamma-ray; the probabilities for alternative decay modes from the nuclear level have been removed.

i) Retardation factor = $T_{\frac{1}{2}}$ (part)/$T_{\frac{1}{2}}$ (Weisskopf) where $T_{\frac{1}{2}}$ (Weisskopf) is given by $0.88A^{-2/3}\ (197/E(keV))^{3}\ 10^{-12}$ sec.

j) The operators for these matrix elements are given in Table I; h = hindered, a = allowed.

k) m = 1 is hindered but the m = 2 penetration contributions are allowed.

m) W^{182} is an even-even nucleus.

The isotopes Hf^{177} and Lu^{175} seemed particularly interesting because the three transitions in each nucleus are related by the rotational model. The three transitions branch from the same intrinsic state to three members of the ground state rotational band.

The two transitions in W^{182}, although the retardation factors are not as large as in the two previous isotopes, are also related by the rotational model. However, W^{182} is an even-even nucleus and the structure of the nuclear states for such nuclei is not as well understood as for the odd A nuclei. The intrinsic states are two particle excitations and the collective vibrational states play a more important role.

Gd^{155} and Tm^{169} also have smaller retardation factors but they nevertheless can be useful as a check on our understanding of the penetration contributions to internal conversion. In both cases the nuclear structure parameters can only be estimated satisfactorily if the second order terms in the expansion of the penetration weighting functions are included.

CHAPTER IV

EXPERIMENTAL INSTRUMENTS AND PROCEDURES

Beta-Ray Spectrometer

The experiments consisted, for the most part, of the measurement of relative conversion electron intensities for each case presented in Chapter III. These measurements were performed on the Caltech $\sqrt{2}\ \pi$ iron free beta-ray spectrometer. This spectrometer has been described very briefly[31] and also more completely in a Caltech report[32].

In this instrument electrons leave the source, travel along the optic circle (35 cm radius), and pass through the exit slits having traversed an angle of $\sqrt{2}\ \pi$. The form of the magnetic field has been determined to produce double focusing with a minimum aberration for sources with a large extent. The advantage of such a field form is that it permits high resolution (the best momentum resolution obtained on this instrument has been 0.02%) with high transmission (0.25% at 0.1% resolution). These focusing properties of the magnetic field allow the use of extended sources (1 mm x 30 mm for 0.1% resolution) thus giving a large luminosity (transmission x source area). The resolution obtainable with a given source depends on the source dimensions and the settings of the spectrometer shutters and slits. These experiments were performed with momentum resolutions varying from 0.04% to 0.2%.

Current was supplied to the spectrometer magnet coils by a 1 kw transistorized power supply. Since high resolution ($\sim$ 4 parts in 10^4) was necessary to perform these experiments the current stability

required was ~ 1 part in 10^5. To achieve this degree of regulation in the current several modifications in the power supply were necessary. The reference section of the supply was redesigned to allow it to be immersed in an oil bath for better temperature control.

Detectors

The detector employed for moderate counting rates was a flow through Geiger-Muller counter. The high stability and efficiency of such counters make them very useful as detectors for beta spectrometers. The G-M counter used for these experiments was designed and built in this laboratory for use specifically with this spectrometer. This was necessary because no extended thin window commercial counters were available.

Under normal conditions a 500 $\mu g/cm^2$ aluminized mylar window was used although formvar windows of 20 - 50 $\mu g/cm^2$ could be used for very low energy work. A commercial gas mixture of 98.7% helium and 1.3% butane was continuously passed through the counter. A plateau of 0.5%/100 volts for a duration of 500 volts was typical for the performance of the counter. Small corrections to the experimental data were occasionally necessary because of the 250 μsec deadtime of the counter. For electron energies less than ~ 70 keV the observed counting rate was corrected for absorption in the counter window.

An anthracene crystal, one meter lightpipe, and phototube assembly were used to handle counting rates of 10^4 cts/sec and more. This counting rate was necessary because several transitions (particularly the 72 and 321 keV transitions in Hf^{177}) were very weak

relative to the intense beta spectrum. The energy dependent back-scattering from the crystal makes this arrangement less desirable for normal operation than the G-M counter.

Sources

All sources used in these experiments were produced by neutron capture at the Materials Testing Reactor at Arco, Idaho. The isotopes sent to the reactor and their abundances were Lu^{176} ($\sim$ 70%), Yb^{168} ($\sim$ 25%), Yb^{174} ($\sim$ 95%), Ta^{181} (100%), and Eu^{153} ($\sim$ 95%). All the sources were in the chemical form of an oxide with the exception of Ta which was a metal.

Upon arrival at Caltech the radioactive material was prepared as beta-ray sources in the following way. The oxide was converted to a fluoride by heating the oxide in hydrofluoric acid. Fluorides were used because rare earth fluorides do not form hydrates. The solution was evaporated to dryness in a platinum boat. The fluoride was evaporated in vacuum from the boat onto 7 mg/cm^2 aluminum foil by passing current through the boat. Strips were cut from the foil and glued on aluminum forms which were carefully mounted in the spectrometer.

To prevent a poor line profile from scattering in the source, it was necessary to make sure the sources were thin. Often several sources were cut and many spectrometer adjustments were made before a reasonably optimized arrangement was obtained. The source strengths of the prepared spectrometer sources were typically Lu^{177} $\sim$ 100 mc, Yb^{169} $\sim$ 0.01 mc, Ta^{182} $\sim$ 0.1 mc, Yb^{175} $\sim$ 1 mc, and Eu^{155} $\sim$ 0.001 mc.

Absolute Conversion Measurements

In addition to measurement of relative electron intensities (relative conversion coefficients) some absolute conversion coefficients were determined. These were determined by comparing the electron and gamma-ray intensities of the transition under study to the electron and gamma-ray intensities of a standard transition with a known conversion coefficient. The Cs^{137} 661 keV transition was used as a standard and the K conversion coefficient was taken to be 0.093 ± 0.003.*) The comparison was made by simultaneously evaporating Cs^{137} and the isotope under study. The electron intensities were compared on the beta spectrometer.

The gamma-ray intensities were compared on a calibrated lithium drifted germanium solid state detector[33]. The efficiency of the germanium detector had been previously determined[34] which allowed relative intensities to be determined to an accuracy of 5% or less. The detector was also used to remeasure the relative gamma-ray intensities in Lu^{175} since conflicting values have been reported in the literature.

Data-Taking Procedure

Intensities of the conversion lines were measured by recording the counting rate as a function of the magnetic rigidity $B\rho$ by automatically advancing over the line profile with a constant step size.

---

*) The value 0.093 represents an approximate average of many measurements reported in the literature. Nearly all these values are in the range 0.090 to 0.095 with errors comparable with the error quoted above.

The observed counting rate is proportional to the number of electrons with momenta between $B\rho$ and $B\rho + \Delta(B\rho)$ where $\Delta(B\rho)$ is the acceptance window of the spectrometer. For this spectrometer $\Delta(B\rho)/B\rho$ is a constant so to obtain relative intensities it is necessary to divide the integrated number of counts in each line profile by the corresponding $B\rho$ for that line.

Two methods were used to automatically advance over the line profile. In the first method the current was advanced with a predetermined step size and a predetermined counting interval (e.g., 150 total steps at 10 min/step), advancing over the line profile only once. In the second method the counting interval was shortened (e.g., to 20 seconds) and the current was recycled over the line profile many times. The print out time was shortened to less than a second by the use of a paper tape punch. The computer was used to combine the data from the many cycles. This recycling of the current was accomplished by placing in the reference section of the power supply a continuous one-turn pot. The pot was advanced with a stepping motor (200 steps/revolution) producing a saw tooth variation in the current, the amplitude of the variation corresponding to the length of the energy region to be recycled. This method for recycling the current is similar to the electromechanical feedback system developed for Mössbauer drives by Kankeleit[35].

The second method was especially useful for measurement of L subshell relative intensities since use of the first method for weak lines might result in a time difference of 2 - 5 days between the L_I and L_{III} lines. In addition to an averaging out of daily variations

in the experimental conditions, the second method also made halflife corrections easier for some of the shorter lived sources (4 and 7 day halflives).

Data Reduction

To obtain the electron intensities the background must be subtracted from the total number of counts. Background counts arise from the normal room background and from the presence of continuous beta spectra in the decay of the parent radio nuclide. This latter factor can be a severe problem for the intensity measurement of a weak transition which is weakly converted. For example, consider the case of the 321 keV L_{III} intensity in Hf^{177}. The beta branching to the 321 keV level is $\sim 10^{-1}$, the gamma-ray branching from the 321 keV level is $\sim 10^{-2}$, $\alpha_{L_{III}}$ is $\sim 10^{-3}$, and the specrometer resolution is $\sim 10^{-3}$. Consequently one expects the ratio of the L_{III} electron intensity to the background to be of the order of 10^{-3}. To insure an accurate determination of the background it was necessary to have a good measurement of the background on both the low and high-energy sides of the peak or peaks.

The raw data is plotted on linear graph paper showing counting rate as a function of $B\rho$. Such a plot is shown in Fig. 1 of the Tm^{169} 63 keV L subshell spectrum. From this plot the background can be determined and then subtracted from the total counting rate. For L subshell spectra the log of the difference is plotted as a linear function of $B\rho$ on semilog paper. Such a plot is shown in the bottom part of Fig. 1. The line profile on such a plot is found to be independent of the line intensity (over a small energy region).

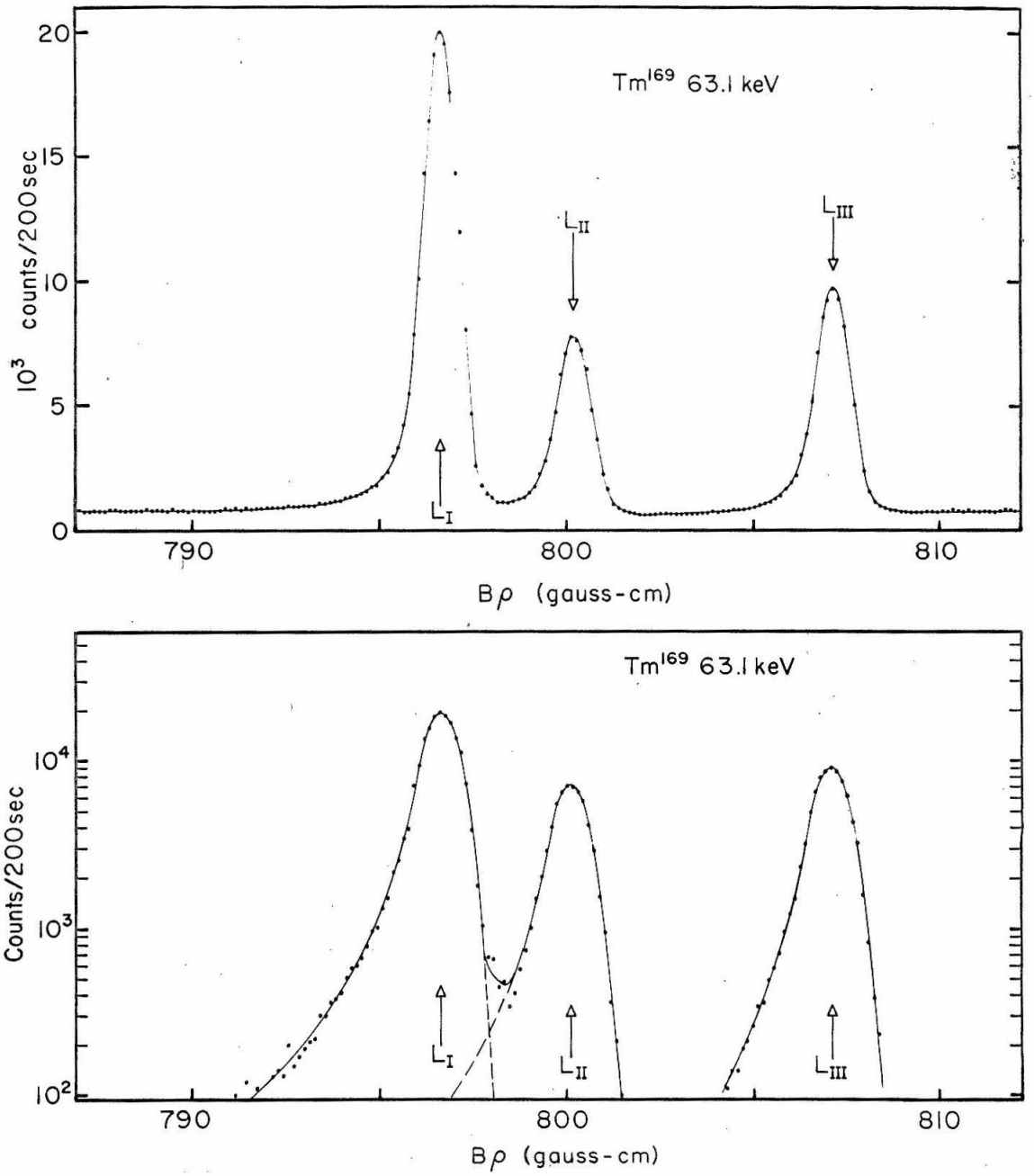

Figure 1.

The L subshell conversion spectrum of the 63 keV transition in Tm^{169} measured at a momentum resolution of 0.15% with the $\sqrt{2}$ π spectrometer. The lower portion of the figure shows a semilog plot of the spectrum after the background counts have been subtracted. The L_{III} line was used to determine the standard line shape which was then used to draw in the profiles for the other two lines.

The line which is least affected by the other lines (usually the L_I) can be used to determine the standard line profile. Using the standard line profile the spectrum can easily be decomposed so that the counts contained in each line can be integrated. Ratios of these intensities are the desired L subshell ratios. For L subshells, heights of the lines may also be compared which is sometimes preferable. The heights are not divided by the corresponding value of $B\rho$.

The intensity of the K conversion line can be obtained, without the aid of the semilog plot, by integration of the counts within the line. Generally, more background is required to obtain the K intensity since the line profile can noticeably flare out on both the low and high energy slides. This results from the increased natural width of the K line ($\sim$ 40 eV compared to $\sim$ 5 eV for the L lines[36]). As pointed out earlier the integrated line intensity must be divided by the corresponding $B\rho$ for that line before it is compared to a different energy line (this is usually negligible for the L subshell lines). Corrections not exceeding 5% for the detector window efficiency and 3% for the detector dead time, as well as for the radioactive decay, were made when required.

For most of the investigated transitions the final experimental numbers (these will be presented in Chapter VI) are the result of more than one measurement. The final results are always a weighted average of all the measurements performed. The errors quoted are generally statistical errors although in cases where a line was not completely resolved from a neighboring line an additional error was added in due to the uncertainty in decomposition of the spectrum.

CHAPTER V

GENERAL REMARKS CONCERNING THE ANALYSIS

Determination of the Experimental λ's

All the cases investigated in this thesis are transitions between non-zero spin states and therefore the possible existence of an M2 admixture cannot be excluded. The E1 transition rates are strongly retarded whereas the M2 rates generally have their dimensional values. When M2 admixtures are considered the conversion coefficient will have the form

$$\alpha(E1 + M2) = \frac{\alpha(E1) + \delta^2\alpha(M2)}{1 + \delta^2}, \qquad (21)$$

where $\alpha(E1)$ and $\alpha(M2)$ are the conversion coefficients for pure multipoles and $\delta^2 = T(M2)/T(E1)$; T is the transition probability. It is important that δ^2 is known since the M2 conversion must be subtracted from the total conversion before the size of the anomaly is determined. Dimensional estimates indicate that the M2 admixture could be as large as a few percent.

δ^2 can be determined from directional correlation experiments or from conversion measurements. In a few of our cases directional correlation experiments have been done but are able to set an upper limit of only 0.02 - 0.05 for δ^2. Conversion measurements can be used to determine δ^2 by comparing the experimental $\alpha_{L_{III}}$ (determined from the experimental α_K and K/L_{III} ratio) with the theoretical E1 and M2 L_{III} coefficients. We are only allowed to do this because the E1 L_{III} conversion coefficient is known to show no anomaly.

Since $\alpha_{L_{III}}(M2)/\alpha_{L_{III}}(E1) \approx 10 - 50$ these measurements are fairly sensitive to the M2 admixture. Such comparisons for our cases give an upper limit for δ^2 of 0 - 0.02. Admixtures of this magnitude have little effect (except possibly for the very small anomalies) on the size of the penetration parameters that are determined from the experiments.

We recall Eq. (13) giving the conversion coefficient in the abbreviated form

$$\alpha_i = \sum_f \text{const.} \left| R_{fi} + \sum_{m=1}^{\infty} (\gamma_m \lambda_m (j\cdot\nabla) + \beta_m \lambda_m (j\cdot r)) \right|^2 . \qquad (13)$$

In order to analyze the experiments we rewrite this in the form

$$\alpha_i = \sum_f \text{const} \left| R_{fi} + \gamma_1 \lambda (j\cdot\nabla) + \beta_1 \lambda (j\cdot r) \right|^2 \qquad (22)$$

where

$$\lambda(j\cdot\nabla) = \lambda_1(j\cdot\nabla) \left(1 + \sum_{m=2}^{\infty} \frac{\gamma_m}{\gamma_1} \frac{\lambda_n(j\cdot\nabla)}{\lambda_1(j\cdot\nabla)} \right) ,$$

$$\lambda(j\cdot r) = \lambda_1(j\cdot r) \left(1 + \sum_{m=2}^{\infty} \frac{\beta_m}{\beta_1} \frac{\lambda_n(j\cdot r)}{\lambda_1(j\cdot r)} \right) . \qquad (23)$$

We will determine the two parameters $\lambda(j\cdot\nabla)$ and $\lambda(j\cdot r)$ from the experiments. These experimentally determined parameters represent the first order terms in the expansion to the extent that the higher order terms can be neglected. Therefore, to obtain $\lambda(j\cdot\nabla)$ and $\lambda(j\cdot r)$ from the experiments we must know R_{fi}, γ_1 and β_1. In order to estimate the importance of the terms with $m \geq 2$ in Eq. (23) we must also know γ_2 and β_2.

In Table III we present the various initial and final electron states involved in E1 conversion in the K, L_I, L_{II}, and L_{III} shells.

TABLE III

INITIAL AND FINAL STATES IN E1 CONVERSION

Initial State			Final State	
Shell	Nonrelativistic Notation	κ_i	Nonrelativistic Notation	κ_f
K, L_I	$s_{1/2}$	-1	$p_{1/2}$	+1
			$p_{3/2}$	-2
L_{II}	$p_{1/2}$	+1	$s_{1/2}$	-1
			$d_{3/2}$	+2
L_{III}	$p_{3/2}$	-2	$s_{1/2}$	-1
			$d_{3/2}$	+2
			$d_{5/2}$	-3

Since the weighting coefficients γ_1 and β_1 are largest for the lowest total angular momentum values, nearly no penetration occurs for the L_{III} $d_{3/2}$ and $d_{5/2}$ final states. Therefore, all penetration contributions from these two partial waves were neglected. The forms of the weighting coefficients γ_1, γ_2, β_1, and β_2 are given in terms of

the electron wave functions in Appendix III. Table XIV in this appendix indicates that β_1 is zero for final states with total angular momentum different from 1/2. In the analysis of the experiments it was assumed that no j·r type of penetration occurs in these partial waves. This is valid because the higher angular momentum of the final states in these partial waves insures that the coefficients $\beta_m (m \geq 2)$ are indeed very small.

To evaluate these weighting coefficients the two lowest order coefficients in the power series expansion about the origin of the initial and final electron radial wave functions are required. These coefficients and also the quantity R_{fi} were obtained by numerical solution of the Dirac equation using a self consistent Hartree potential taking into account exchange in the Slater free-electron approximation. The potential inside the nucleus was taken to be that resulting from a uniform isotropic charge distribution. This calculation is described briefly[37] and also more completely in the work reported by E. Seltzer[38] who was largely responsible for the success of these calculations.

The radial integrals R_{fi} are, of course, complex although the imaginary part is always quite dominant. Since the penetration contributions are pure imaginary there will be strong interference between R_{fi} and the penetration terms. It is therefore possible that the conversion coefficient will increase or decrease in size due to the penetration terms.

Because Eq. (22) is quadratic in λ two solutions for λ are obtained for a given measurement. Generally, several measurements will be consistent for only one of the two solutions although in some cases

both solutions are consistent with the experiments. In this case the solution was taken for which $\lambda(j\cdot\nabla) \approx 0$ (the other solution was always for $\lambda(j\cdot\nabla) \gg 1$) in view of the dimensional estimate in Eq. (16).

Theoretical Estimates for the λ's

The nuclear structure parameters $\lambda(j\cdot r)$ and $\lambda(j\cdot\nabla)$ can only be calculated within the framework of a nuclear model. The unified model as outlined in Chapter II was used as the basis for such estimates.

The gamma-ray matrix element $\langle f||rY_1^*||i\rangle$ was determined from the experimental E1 lifetime through use of the formula[20]

$$\langle f||rY_1^*||i\rangle = 9.0 \times 10^{-3}\, e_{eff}\sqrt{\frac{M\omega\,(2I_i+1)}{E^3(\mathrm{MeV})\,T_{1/2}(\mathrm{sec})}}\,, \qquad (24)$$

where M is the nucleon mass, ω is the oscillator shell spacing energy, E is the transition energy, $T_{1/2}$ is the E1 halflife, and e_{eff} is the effective charge equal to Ne/A for a proton and -Ze/A for a neutron[39]. I_i is the angular momentum of the initial state. The sign of the matrix element is indeterminate because of the square root. These matrix elements are very small relative to their unhindered values and consequently these quantities cannot be calculated with reliability using any of the presently developed nuclear models. These calculations generally involve cancellation to a few percent and so not even the sign is certain.

An interesting point arises in consideration of the gamma-ray matrix element. The gamma-ray matrix element $\int j\cdot A_{1M}^*$ is usually very well represented by the long wavelength approximation

$$\int j \cdot A^*_{1M} = \text{const.} \int j \cdot \nabla \, r \, Y^*_{1M}$$

Equation (47) of Appendix II indicates that the higher order terms in the matrix element for gamma-ray emission are just the penetration matrix elements as defined earlier. This equation written in terms of the nuclear structure parameters has the form

$$\int j \cdot A^*_{1M} = \sqrt{2} \, \frac{R}{3} \int j \cdot \nabla \left(\frac{r}{R} \right) Y^*_{1M} \left[1 + (kR)^2 \left(\lambda_1 (j \cdot r) - \frac{1}{5} \lambda_1 (j \cdot \nabla) \right) + \ldots \right] . \tag{26}$$

Although the higher order terms are weighted by $(kR)^2$ which is of the order of 10^{-4}, the retardation of the gamma-ray transition probability could be large enough so that the higher order terms cannot be neglected. We will see later that for two transitions $\lambda(j \cdot r) \approx 10^3$ and consequently these higher order terms cause a 10 - 20% correction to the usual gamma-ray matrix element. To our knowledge these experiments demonstrate for the first time that such terms contribute significantly to the gamma-ray transition probability.

The penetration matrix elements were calculated for m = 1 and 2 using the operators presented in Table I for the odd mass nuclei. Rassey wavefunctions[40] were used with the deformation parameter ϵ equal to 0.3. The wave functions calculated by Rassey are identical to the more familiar Nilsson wave functions[22] except they are represented in terms of asymptotic basis states instead of spherical basis states. The m = 1 and 2, spin and convection current contributions were combined using Eq. (23) to give the theoretical estimate for $\lambda(j \cdot r)$. The terms for $m \geq 3$ are expected to contribute

only a few percent at most to this estimate.

For μ (the magnetic moment of the nucleon) the effective values of 2 for protons and -1.2 for neutrons[14] were used. These values are in rough agreement with the data on magnetic moments[41,42]. This quenching of the magnetic moment results from a spin polarization of the core due to the single particle.

The contributions to the nuclear current from the $\vec{\ell}\cdot\vec{\ell}$ and $\vec{\ell}\cdot\vec{s}$ terms in the Hamiltonian (see Eq. (20)) were neglected. This is completely valid for the j·r matrix elements since the resulting current has no radial components. Although the $\vec{\ell}\cdot\vec{\ell}$ and $\vec{\ell}\cdot\vec{s}$ terms may give non-zero contributions to the j·∇ matrix elements we will not be concerned with them since the j·∇ terms will later be seen to be unimportant in the analysis.

According to the rotational model the reduced matrix elements for gamma-ray transitions of the same multipolarity L between states of two rotational bands are related simply by Clebsch-Gordan coefficients. This relation is given by[21]

$$\frac{\langle I_f||O_L||I_i\rangle}{\langle I_f'||O_L||I_i'\rangle} = \frac{(I_i L\ K_i \Delta K|I_f\ K_f)}{(I_i' L\ K_i \Delta K|I_f'\ K_f)}\ , \qquad (27)$$

where I_i and I_i' refer to the two initial states in the rotational band K_i; I_f and I_f' refer to the two final states in the rotational band K_f. This relation allows us to compare the λ's for two such transitions. If we assume the allowed penetration matrix elements M_p obey the above collective branching rule and again predict the gamma-ray matrix elements M_γ from experiment then

$$R = \frac{\lambda}{\lambda'} = \frac{M'_\gamma}{M_\gamma} \frac{M_p}{M'_p} \sqrt{\frac{Y'}{Y} \left(\frac{E}{E'}\right)^3 \left(\frac{C}{C'}\right)^2} \quad , \tag{28}$$

where Y is the experimental gamma-ray intensity, E is the transition energy, and C is the Clebsch-Gordan coefficient appearing in Eq. (27). Before such a comparison can be made the energy dependence must be removed from the experimentally determined $\lambda(j \cdot r)$. Of course, the sign of R cannot be predicted since the sign of M_γ is unknown.

The unified model as used here does not take into account the effects of pairing correlations between nucleons[19,43]. When these effects are accounted for it can be shown[44] that the theoretical transition probability between two single particle states can be written in the form

$$T = T_0 F, \tag{29}$$

where T_0 is the usual single particle transition probability and F is a reduction factor due to the pairing correlations. F can be written as

$$F \approx (U_i U_f - \tau V_i V_f)^2. \tag{30}$$

U_i^2 and V_i^2 are the respective probabilities to find the initial level empty or occupied by a pair of particles. The subscript f refers to the final level. The factor τ is determined by the time-reversal properties of the single particle operator. For operators even under time reversal $\tau = +1$ and for operators odd under time reversal $\tau = -1$.

The usual electric multipole operator $r^L Y_{LM}$ is even under

time reversal and so for the gamma-ray matrix elements $\tau = +1$. Consequently cancellation is possible in F and the theoretical transition probability could be reduced by 10 - 1000[45-47] because of F. This has frequently been used as a cause for the large E1 retardation factors. Unfortunately, the quantities U and V cannot be computed with reliability so quantitative conclusions are difficult to make.

The $j \cdot \nabla$ type of penetration matrix element also has $\tau = +1$. and so here too a significant reduction can occur due to the pairing correlations. However, the $j \cdot r$ type of penetration matrix element is odd under time reversal and consequently the reduction factor F is likely to be close to unity. This is certainly fortunate in terms of these experiments, since a small F would probably make all penetration terms unobservable.

CHAPTER VI

DISCUSSION OF THE CASES

Lu^{175}

The decay scheme of $Yb^{175} \rightarrow Lu^{175}$ is shown in Fig. 2. The nuclear levels are labeled by the quantum numbers $I\pi K[Nn\Lambda]\Sigma$. Anomalies were observed for the three E1 transitions which branch from the 396 keV level.

Figure 3 shows the spectrum of the 396 keV L subshell conversion lines. The first spectrum was run at high resolution to obtain the L_I/L_{II} ratio and the second was at poorer resolution to obtain the $(L_I + L_{II})/L_{III}$ ratio. Figure 4 and Fig. 5 show the spectra of the 282 and 144 keV L subshell conversion lines. The spectrum of the 144 keV lines was difficult to measure because the electron intensities are rather weak. No intensity was determined for the L_{III} since it was impossible to resolve from the 137 keV M lines. Figure 6 shows the gamma-ray spectrum measured with the lithium drifted germanium detector. The L subshell ratios, absolute conversion coefficients, and relative gamma-ray intensities determined from these measurements are given in Table IV. The numbers in parentheses are the theoretical numbers taken from the calculations of Seltzer[38].

Figure 7 shows $\lambda(j \cdot r)$ as a function of $\lambda(j \cdot \nabla)$ for the 396 keV transition assuming no M2 admixture. For a given measurement (e.g., α_K) each of the two regions which explain that measurement are contained within a band, the edges of the band representing the limits of experimental error. The solutions obtained for all three L subshell

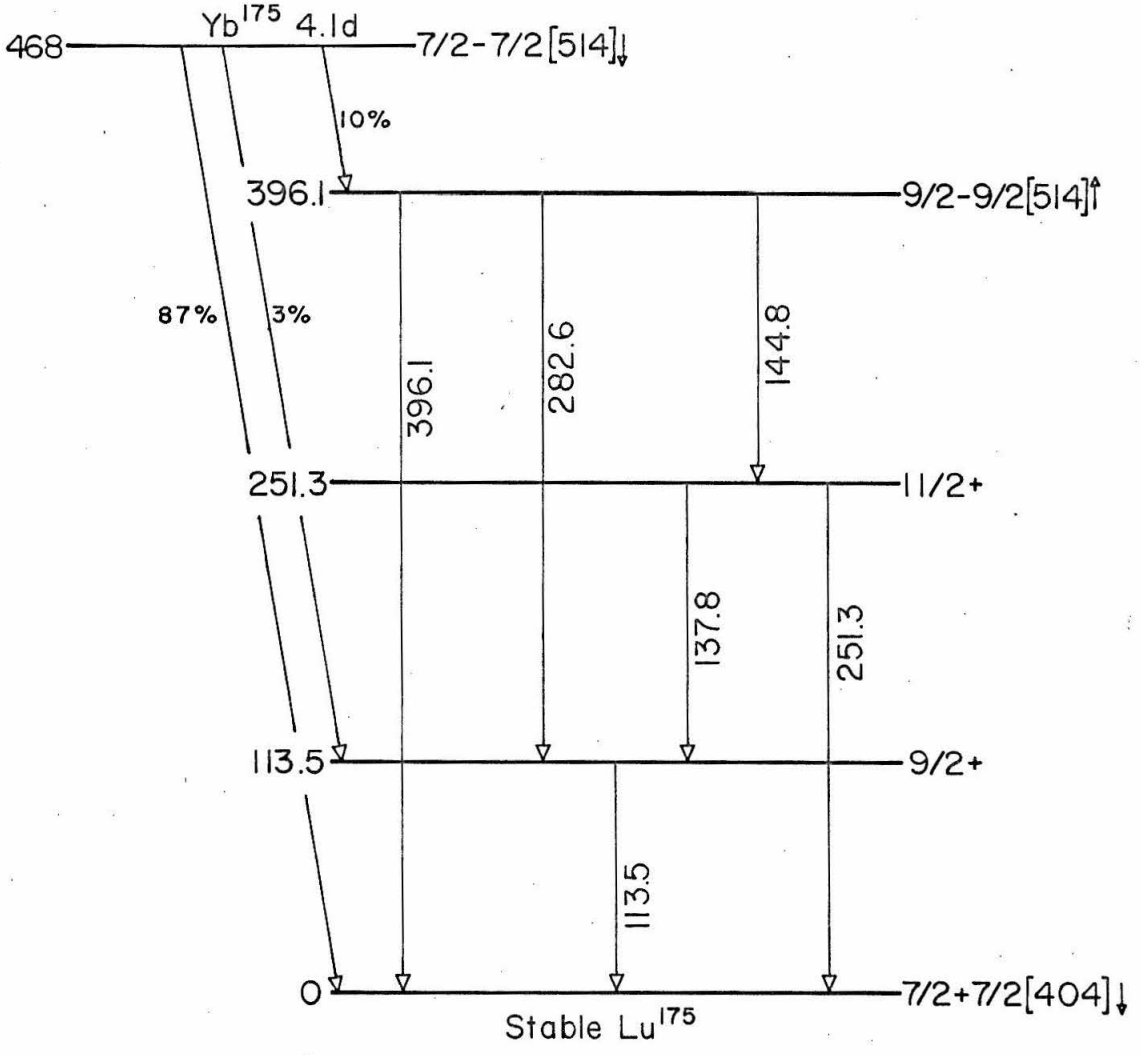

Figure 2.

The decay scheme of $Yb^{175} \rightarrow Lu^{175}$. The levels are labeled by the quantum numbers $I\pi K[Nn\Lambda]\Sigma$. The excitation and transition energies are expressed in keV.

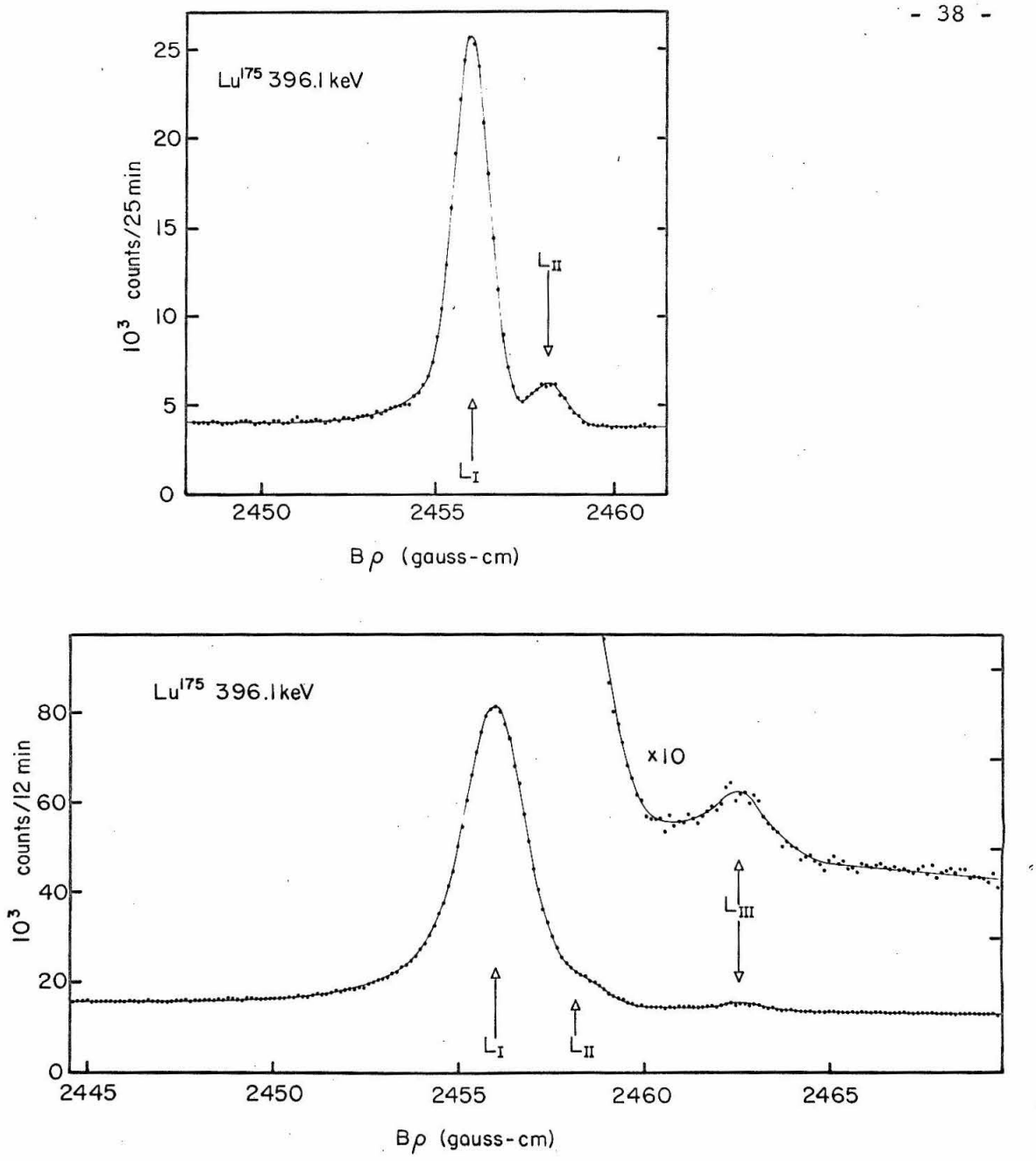

Figure 3.

The L subshell conversion spectrum of the 396 keV transition in Lu^{175} measured with the $\sqrt{2}$ π spectrometer. The L_I/L_{II} ratio was obtained from the upper spectrum measured at 0.04% momentum resolution. The $(L_I + L_{II})/L_{III}$ ratio was obtained from the lower spectrum measured at 0.08% resolution. Using the scale on the right the L_{III} is enlarged by a factor of ten.

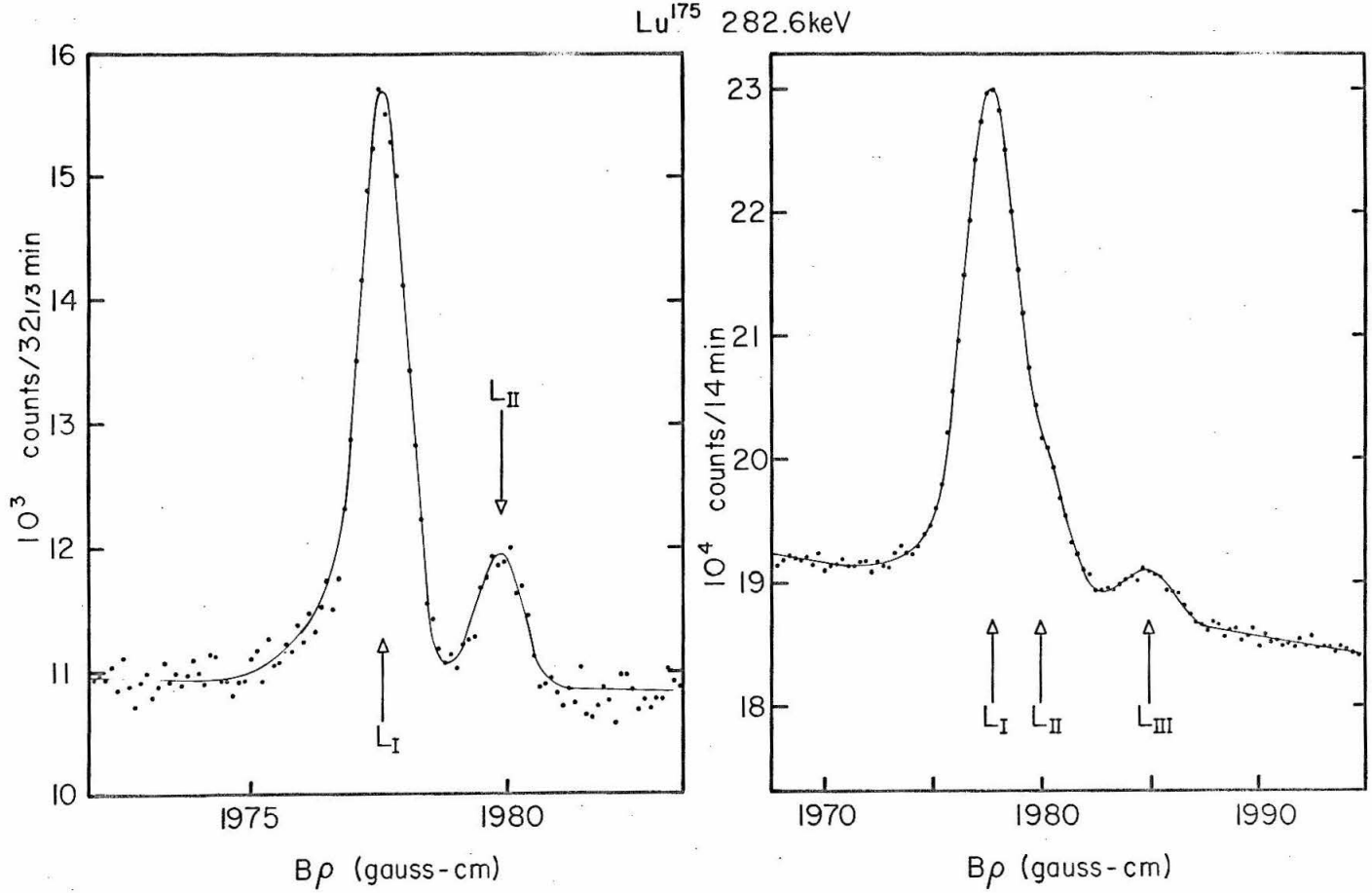

Figure 4

The L_I subshell conversion spectrum of the 282 keV transition in Lu^{175} measured with the $\sqrt{2}$ π spectrometer. The L_I/L_{II} ratio was obtained from the spectrum on the left measured at 0.06% momentum resolution. The $(L_I + L_{II})/L_{III}$ ratio was obtained from the spectrum on the right measured at 0.14% resolution.

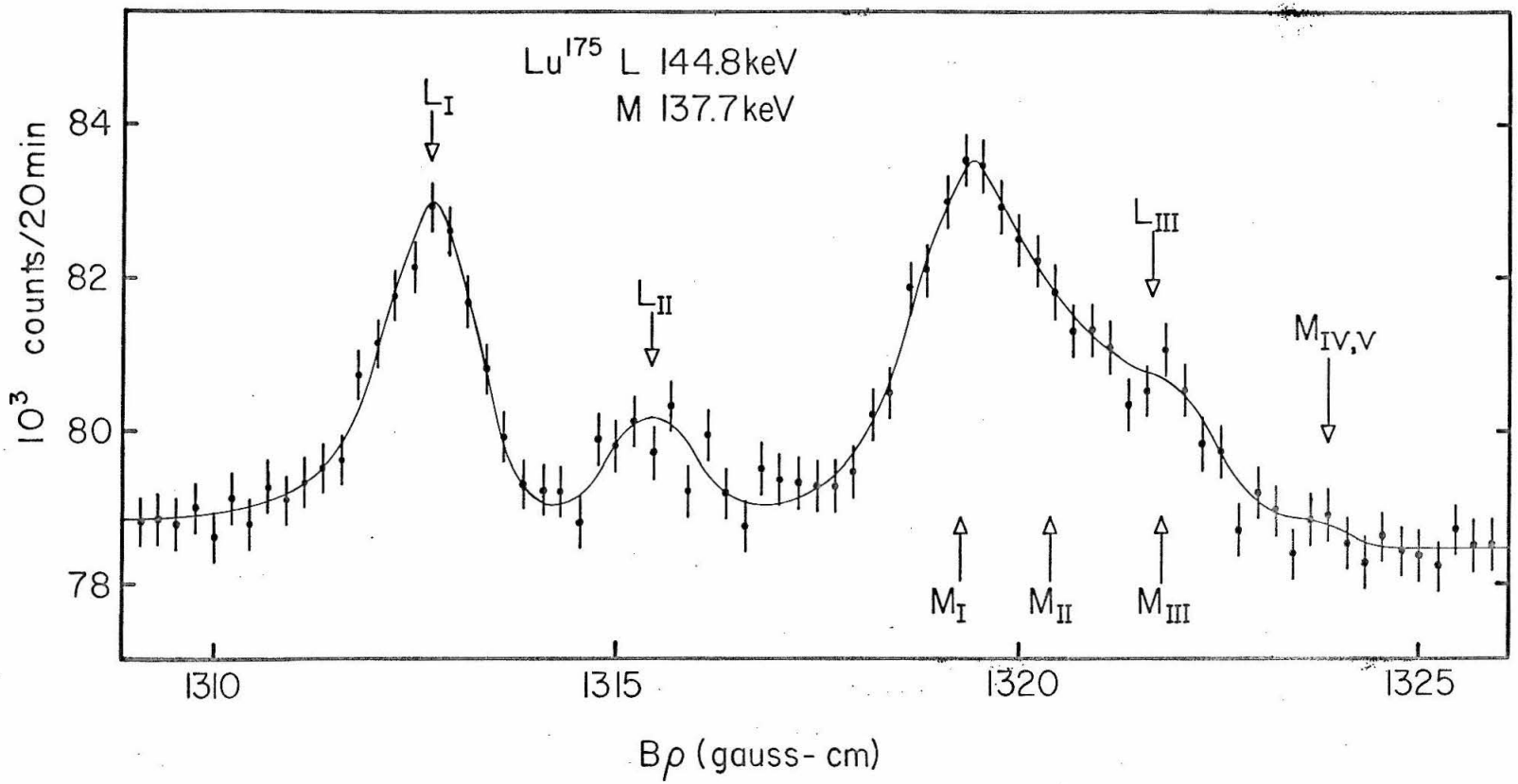

Figure 5.

The L subshell conversion spectrum of the 144 keV transition in Lu^{175} measured at 0.13% momentum resolution with the $\sqrt{2}$ π spectrometer. The L_{III} line was not resolved from the 137 keV M shell conversion lines.

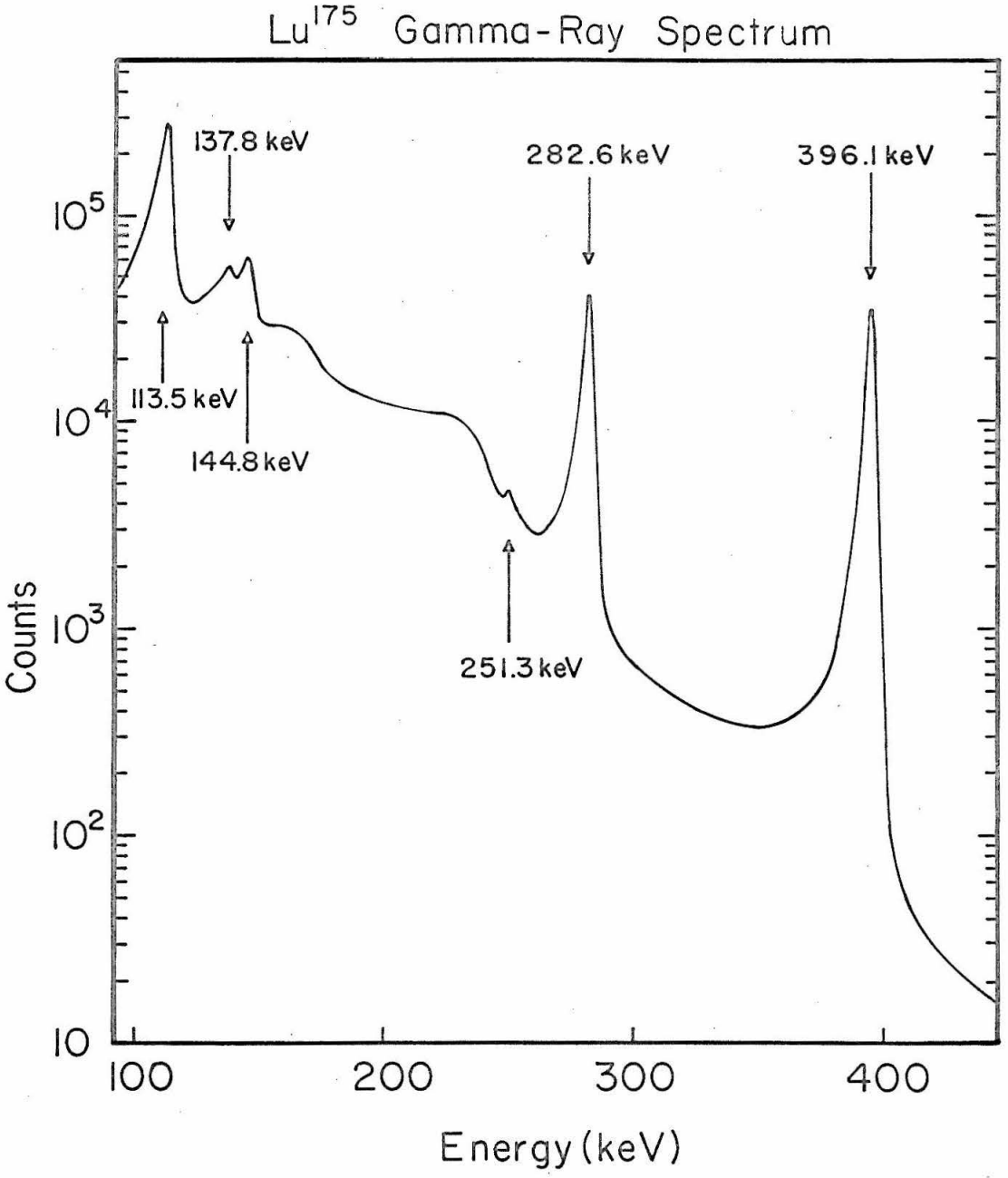

Figure 6

The gamma-ray spectrum of Lu^{175} measured with the lithium drifted germanium detector.

TABLE IV

EXPERIMENTAL CONVERSION AND GAMMA-RAY INTENSITIES IN Lu^{175}

Energy (keV)	Gamma-Ray (Relative Units)	α_K	L_I/L_{II}	L_I/L_{III}	L_{II}/L_{III}
396.1	100	0.037 ± 0.002 (0.0091)	9.2 ± 0.2 (9.2)	53 ± 3 (9.8)	5.8 ± 0.3 (1.1)
282.6	48 ± 2	0.022 ± 0.001 (0.020)	4.3 ± 0.2 (7.3)	10.5 ± 0.6 (7.5)	2.44 ± 0.16 (1.0)
144.8	5.5 ± 0.4	0.084 ± 0.006 (0.111)	3.2 ± 0.6 (4.6)	α_{L_I} = 0.0087 ± 0.0008 (0.0124)	

a) The theoretical values in parentheses were obtained from the calculations described in Ref. 38.

ratios are shown even though only two ratios are independent, i.e., if two L subshell ratio solutions coincide in some region then the third subshell ratio must necessarily give a solution in agreement with the other two ratios. The graph shows that there are two regions where all the measurements are explained by a single set of λ's. As outlined earlier the solution with a large value of $\lambda(j\cdot\nabla)$ was excluded. A complex solution for $\lambda(j\cdot r)$ is indicated by an asterisk on the graph.

Figure 8 shows a graph of $\lambda(j\cdot r)$ as a function of δ^2 for two different values of $\lambda(j\cdot\nabla)$. This graph indicates that $\lambda(j\cdot r)$ depends only weakly on δ^2 although agreement seems best for $\delta^2 < 0.02$. Using our experimental α_K and K/L_{III} ratio, we require

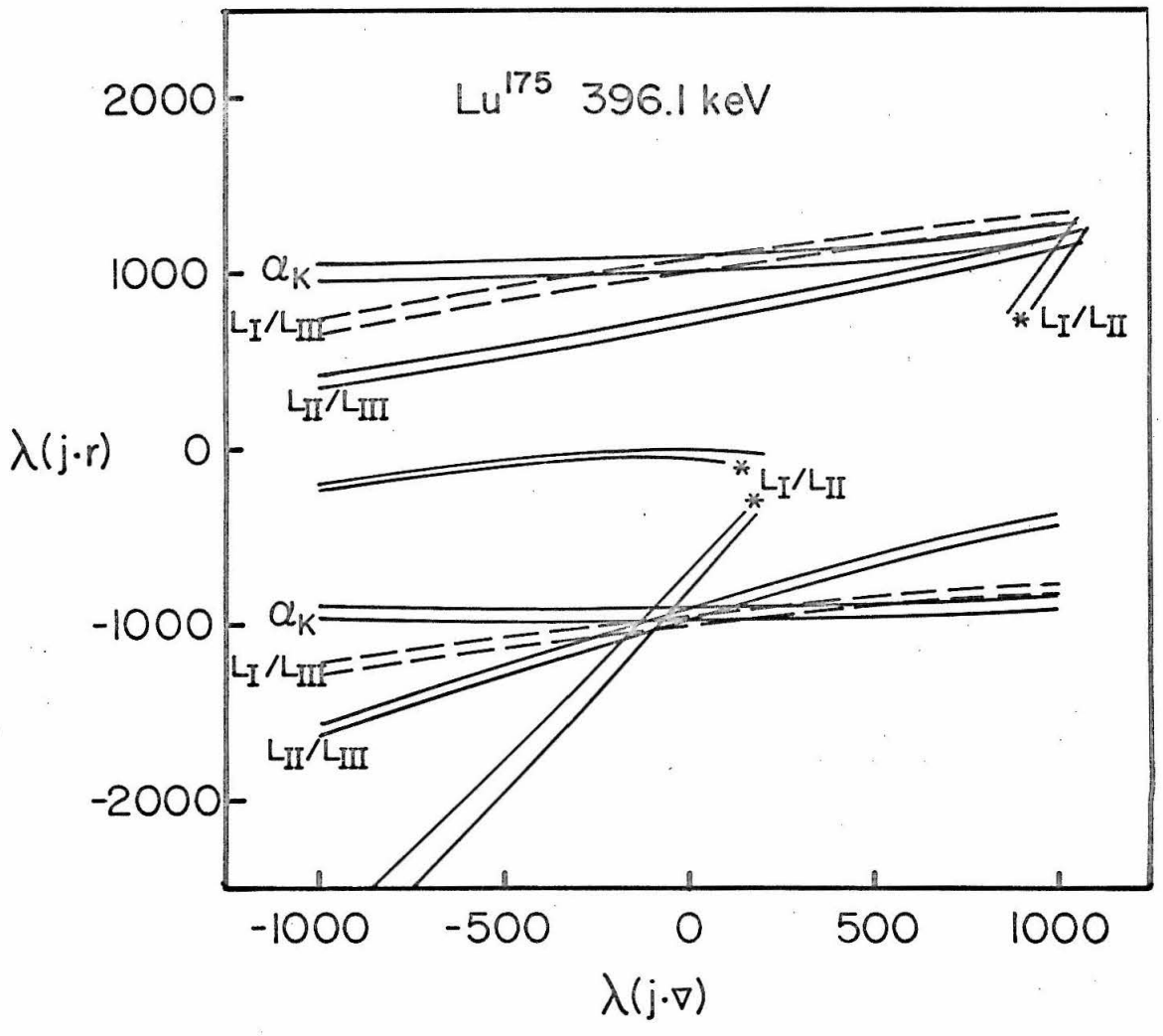

Figure 7.

$\lambda(j\cdot r)$ as a function of $\lambda(j\cdot\nabla)$ for the 396 keV transition in Lu^{175} determined from the various measurements. For a given measurement (e.g., α_K) the values of $\lambda(j\cdot r)$ and $\lambda(j\cdot\nabla)$ which explain that measurement are contained within a band, the edges of the band representing the limits of experimental error. Both solutions of the quadratic equation are shown. This analysis was done assuming no M2 admixture. The asterisk indicates where $\lambda(j\cdot r)$ becomes complex.

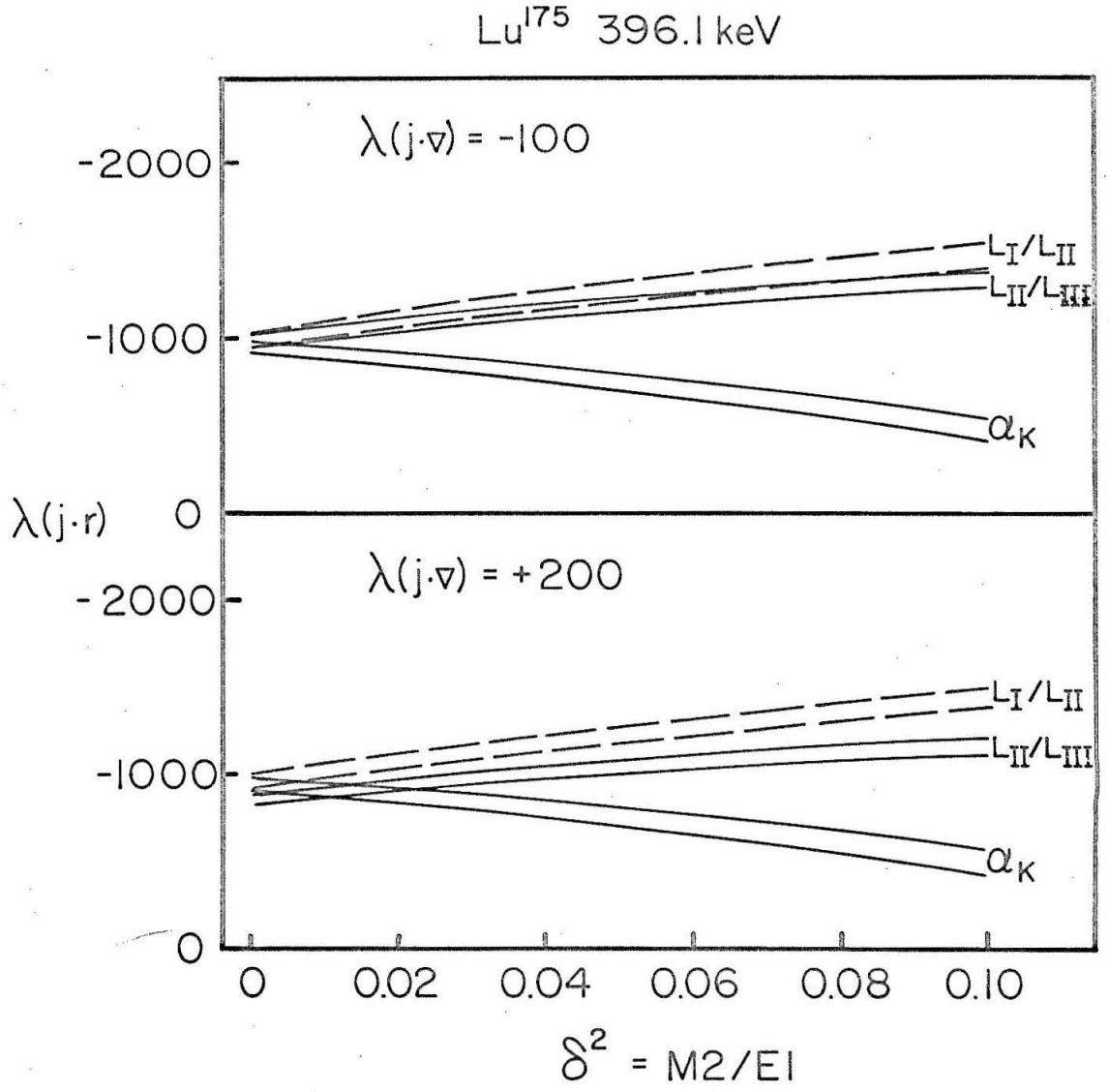

Figure 8

The variation of $\lambda(j\cdot r)$ with $\delta^2 = M2/E1$ for the 396 keV transition in Lu^{175} with $\lambda(j\cdot\nabla) = -100$ (top) and $\lambda(j\cdot\nabla) = +200$ (bottom). For a given measurement (e.g., α_K) the values of $\lambda(j\cdot r)$ and δ^2 which explain that measurement are contained within a band, the edges of the band representing the limits of experimental error.

$\delta^2 < 0.015$. Using the unified model to calculate the allowed M2 transition rate and using the experimental E1 transition rate we find $\delta^2 = 0.001$. Since δ^2 is expected to decrease with decreasing transition energy, we certainly seem justified in disregarding the small M2 admixtures that are possible for all three transitions.

In the graph of $\lambda(j\cdot r)$ vs $\lambda(j\cdot\nabla)$ for the 282 keV transition (Fig. 9) the results of the particle parameter*) experiment by Thun et al.[49] have been analyzed in addition to our results. The theoretical K electron particle parameter $b_2(e_K)$ is defined as[50]

$$b_2(e_K) = 1 - \frac{|2 + T_e|^2}{2 + |T_e|^2} \quad , \tag{31}$$

where

$$T_e = e^{i\epsilon} \frac{R_\kappa = +1}{R_\kappa = -2} \quad . \tag{32}$$

---

*) If one measures the angular correlation between two cascading gamma rays, one finds

$$\omega(\theta_{12}) = \sum_{n=0}^{N} f_{2n}(1)\ f_{2n}(2)\ P_{2n}(\theta_{12})$$

where the f's are tabulated theoretical factors. A complete description is given by Frauenfelder and Steffen[48]. If now the correlation between the gamma ray of transition 1 and a conversion electron of transition 2 is measured, one finds

$$\omega(\theta_{12}) = \sum_{n=0}^{N} f_{2n}(1)\ b_{2n}(2)\ f_{2n}(2)\ P_{2n}(\theta_{12}),$$

where b_{2n} are the particle parameters. They can be determined experimentally by comparing the gamma-gamma and gamma-electron angular distributions.

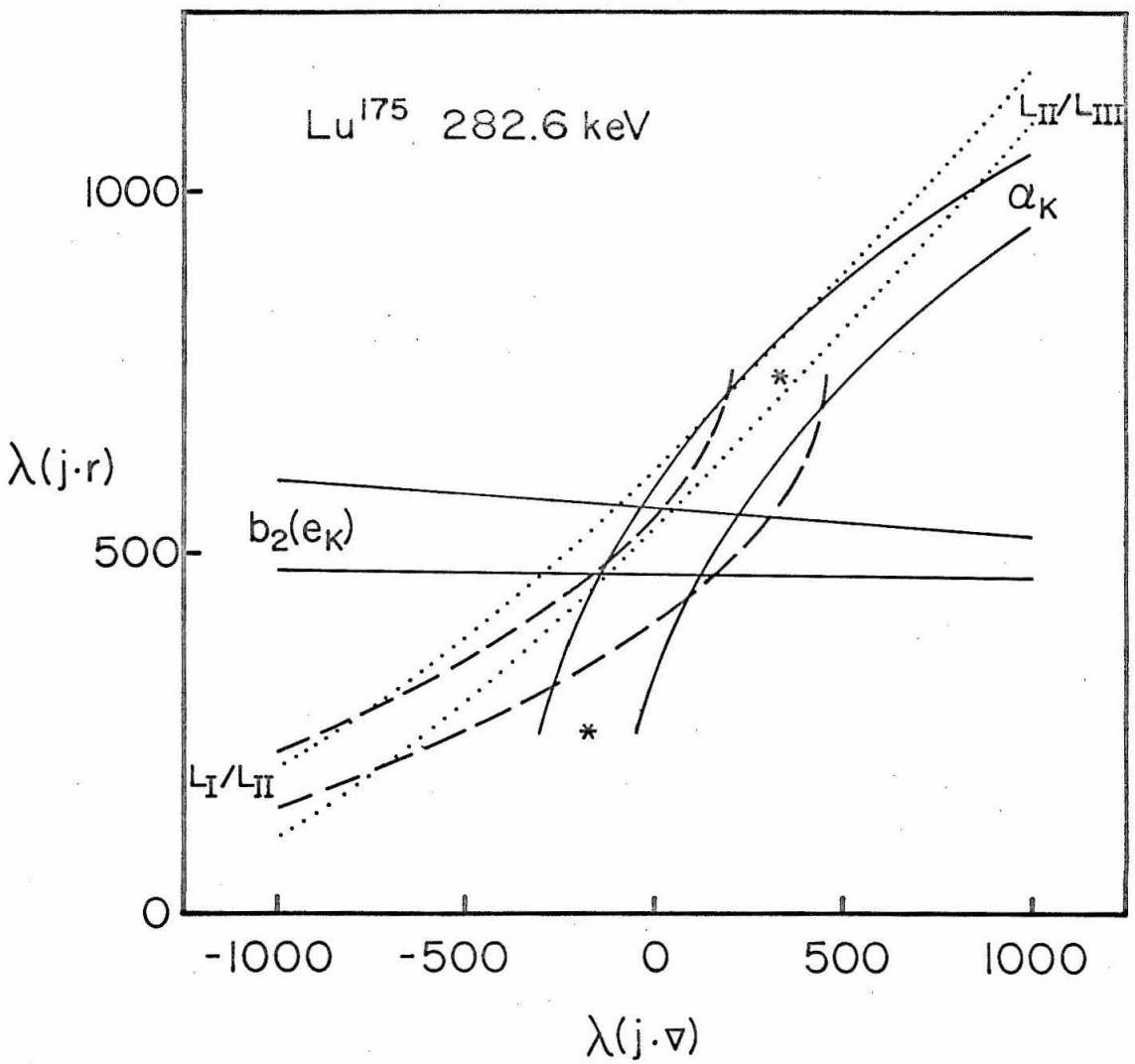

Figure 9

$\lambda(j\cdot r)$ as a function of $\lambda(j\cdot\nabla)$ for the 282 keV transition in Lu^{175} determined from the various measurements. For a given measurement (e.g., α_K) the values of $\lambda(j\cdot r)$ and $\lambda(j\cdot\nabla)$ which explain that measurement are contained within a band, the edges of the band representing the limits of experimental error. The experimental particle parameter $b_2(e_K)$ measured by Thun et al.[48] was also analyzed and the results are shown. The second solution of $\lambda(j\cdot r)$ is not shown because the particle parameter result is not consistent with the conversion results. The analysis was done assuming no M2 admixture. The asterisk indicates where $\lambda(j\cdot r)$ becomes complex.

R_{+1} and R_{-2} are the same electron radial integrals which enter into the K conversion coefficient, $\alpha_K = \text{const}\,[|R_{+1}|^2 + 2|R_{-2}|^2]$, and ϵ is the phase difference between the two final state electron wave functions. Of course, by R we imply that penetration effects must be included when they are significant.

By comparing either the experimental $b_2(e_K)$ or α_K with the corresponding theoretical quantity we are able to determine $\lambda(j\cdot r)$, neglecting $\lambda(j\cdot\nabla)$ for the moment. Since the dependence of α_K and $b_2(e_K)$ on R_{+1} and R_{-2} is different one of these quantities may be much more useful to observe small penetration effects, although it must be remembered that one measurement alone does not determine λ because the equations are quadratic. This is borne out by noting that the value of 500 for $\lambda(j\cdot r)$ indicated in Fig. 9 causes α_K to increase by 10% whereas $b_2(e_K)$ changes from - 1.52 to + 0.06 ± 0.12. The graph also indicates that the particle parameter measurement and one conversion measurement determine the penetration parameters much better than any number of conversion measurements without the particle parameter measurement. Only one solution is shown in Fig. 9 because for the second solution the particle parameter measurement yields a value of $\lambda(j.r)$ which is inconsistent with the value obtained from the conversion measurements. Since only one solution is consistent with the measurements, we have experimental evidence for this case that $\lambda(j\cdot\nabla) < \lambda(j\cdot r)$.

Figure 10 showing $\lambda(j\cdot r)$ vs $\lambda(j\cdot\nabla)$ for the 144 keV transition indicates a more uncertain situation. The absolute conversion measurements α_K and α_{L_I} can only be explained with $\lambda(j\cdot\nabla) \gtrsim 200$ which

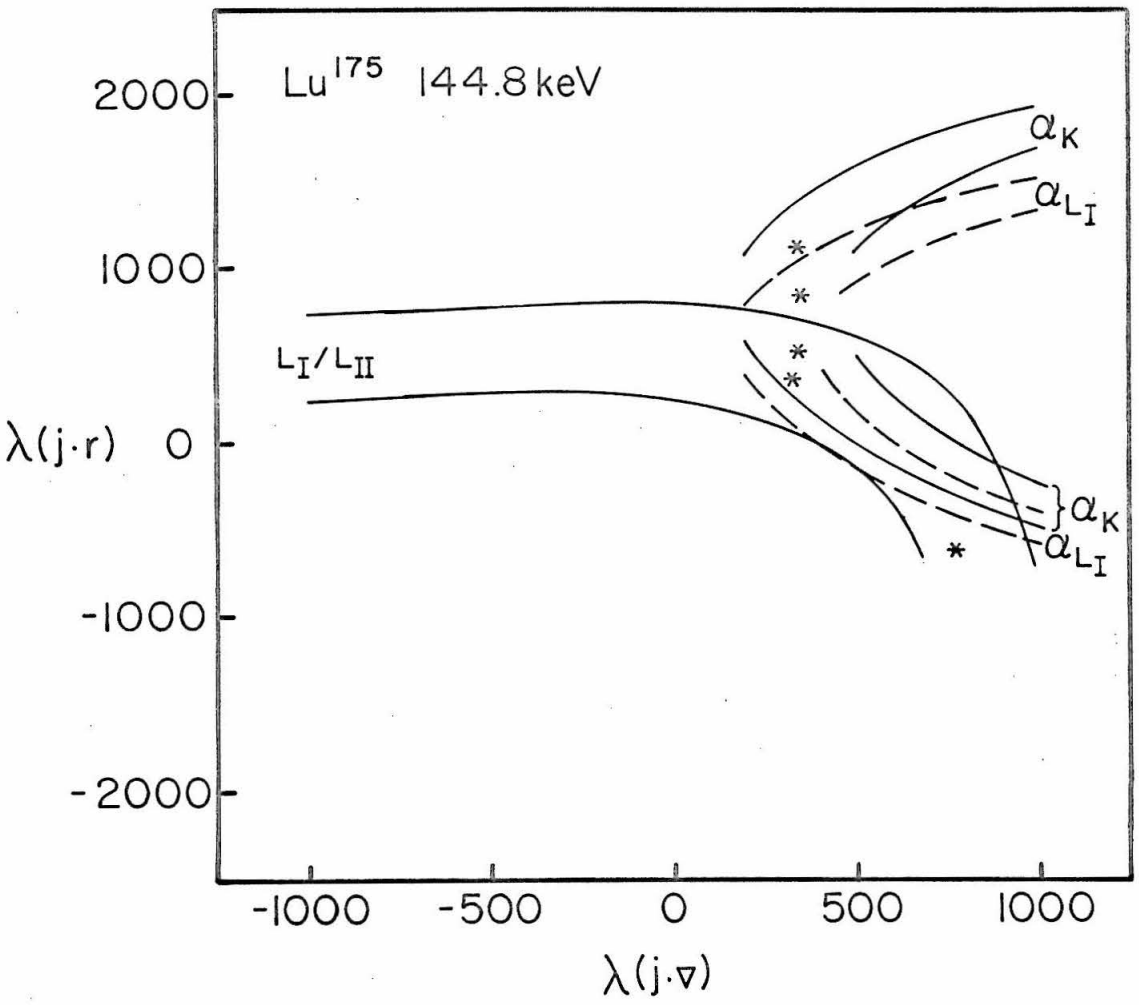

Figure 10

$\lambda(j\cdot r)$ as a function of $\lambda(j\cdot\nabla)$ for the 144 keV transition in Lu^{175} determined from the various measurements. For a given measurement (e.g., α_K) the values of $\lambda(j\cdot r)$ and $\lambda(j\cdot\nabla)$ which explain that measurement are contained within a band, the edges of the band representing the limits of experimental error. The second solution of $\lambda(j\cdot r)$ for the L_I/L_{II} measurement is not shown because it excludes all but extremely large values of $\lambda(j\cdot r)$. No M2 admixture was assumed and the asterisk indicates where $\lambda(j\cdot r)$ becomes complex.

is inconsistent with the dimensional estimates described earlier. In contrast with the 282 and 396 keV transitions, the measured absolute conversion coefficients for the 144 keV transition are smaller than the theoretical values (by ~ 25%). Since $\lambda(j \cdot r)$ enters only in a partial wave which contributes ~ 15% of the total conversion coefficient, it is impossible to decrease the theoretical conversion coefficient by more than this 15% when only $\lambda(j \cdot r)$ is used in the analysis (i.e., $\lambda(j \cdot \nabla) = 0$). We have chosen to disregard the measurements of α_K and α_{L_I} since if they were in error by only 10% the curves in Fig. 10 would shift to the left enough to include $\lambda(j \cdot \nabla) = 0$. They would then still be consistent with the L_I/L_{II} measurement. In general, the relative L subshells, separated only by a few keV in energy, are much easier to reliably measure than the absolute conversion coefficients which usually involve large energy separations and a knowledge of the relative gamma-ray intensities.

It is apparent that the lower energy transitions seem to show much less anomaly for a given size of $\lambda(j \cdot r)$. A λ of - 1000 for the 396 keV transition causes the absolute conversion to increase by a factor of 4 but a λ of 500 for the 144 keV transition causes changes only of the order of 20%. This trend is shown in Fig. 11 which indicates the size of $\lambda(j \cdot r)$ required to increase α_K by 10%.

The values of the experimentally determined λ's are given in Table V. The theoretical first and second order contributions to $\lambda(j \cdot r)$ from the spin and convection currents are given for the 396 keV transition. The retarded convection current contributions

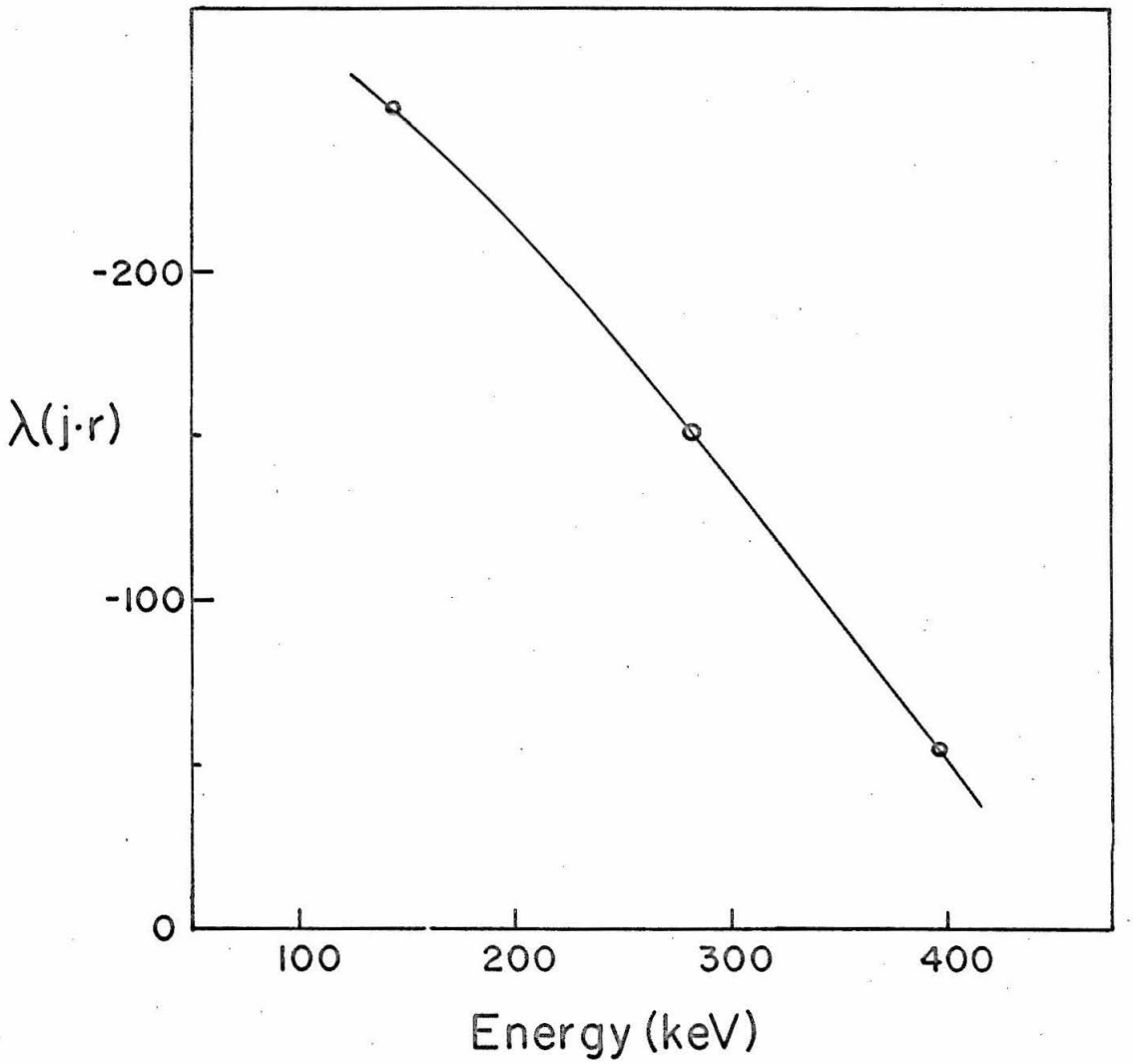

Figure 11

The size of $\lambda(j \cdot r)$ required to increase α_K by 10% as a function of the transition energy in Lu^{175}. The line was drawn through the three points to indicate the trend.

TABLE V

EXPERIMENTAL AND THEORETICAL PENETRATION PARAMETERS FOR Lu^{175}

Energy (keV)	$\lambda(j\cdot r)$ (exp)	$\lambda(j\cdot r)$ (theo)				
		Spin a)		Convect. b)		Total c)
		λ_1	λ_2	λ_1	λ_2	
396.1	-1000 ± 100	2100	1900	50	10	2100

Energy (keV)	$\lambda(j\cdot r)$ (exp)	$\frac{\lambda(E)}{\lvert\lambda(396)\rvert}\left(\frac{E}{396}\right)$ d)	R e)	Sign of M_γ f)
396.1	-1000 ± 100	- 1.0	1.0	-
282.6	500 ± 100	0.35 ± 0.07	0.42	+
144.8	500 ± 250	0.2 ± 0.1	0.14	+

a) Calculated using the second term of the second equation in (15).

b) Calculated using the first term of the second equation in (15).

c) Calculated using the second equation of (23) neglecting the terms for $m \geq 3$. Since β_1/β_2 is very close to - 7 this sum is just $\lambda_1(j_s\cdot r) + \lambda_1(j_c\cdot r) - (1/7)(\lambda_2(j_s\cdot r) + \lambda_2(j_c\cdot r))$.

d) The experimentally determined $\lambda(j\cdot r)$ normalized to 1.0 for the 396 keV transition. The λ's are multiplied by the transition energy to remove all energy dependence.

e) Calculated from Eq. (28) where the prime refers to the 396 keV transition.

f) Sign of the gamma-ray matrix element determined from the sign of

the experimentally determined $\lambda(j\cdot r)$ taking the sign of the penetration matrix element from the theoretical calculation.

are more than an order of magnitude smaller than the allowed spin current contributions. The ratio λ_1/λ_2 for the spin current is ~ 1 but the nearly energy independent ratio of the weighting coefficients β_1/β_2 is ~ -7 and consequently λ_2 makes only a 15% correction to λ_1. A comparison of the total theoretical estimate of 1900 with the experimental value of -1000 tells us that the theoretical estimate is roughly two times too large and that the gamm-ray matrix element must be negative. The agreement seems good in view of the uncertainty represented by the core polarization and the pairing correlation factor $(U_iU_f + V_iV_f)$.

Column 3 of the lower portion of the table gives the experimental ratio $\lambda(E)/|\lambda(396)|\ (E/396)$. The factor E/396 is included to remove the energy dependence from $\lambda(j\cdot r)$ (see Eq. (15)). These entries are to be compared with the branching predictions of the rotational model listed under R. The agreement seems to be very good indeed.

The upper limit of 200 for $\lambda(j\cdot\nabla)$ determined for the 396 and 282 keV transitions is not given in the table. This number is to be compared with the theoretical estimate of 0.3. This suggests that the analysis can be adequately carried out without introducing the $j\cdot\nabla$ type of penetration terms.

Since we know now the sign of the gamma-ray matrix elements we can attempt to understand the E1 gamma-ray transitions rates.

Table VI indicates that the estimates using the branching rules of the rotational model are certainly not in agreement with the experimental branching ratios, the most noticeable disagreement being the sign of the 396 keV matrix element. Cancellation between terms of the intrinsic E1 matrix element reduces the estimate by a factor of ~ 20 making the transition probabilities very sensitive to the details of the wave function. Thus there seems to be considerable evidence for K impurities in the wave functions.

TABLE VI

CONTRIBUTIONS TO GAMMA-RAY MATRIX ELEMENTS IN Lu^{175}

Origin of Contribution	Estimates of Reduced Matrix Element (Relative Units)		
	$I_f = 7/2$	$I_f = 9/2$	$I_f = 11/2$
Expt.	-1.5	1.8	1.6
Expt. a)	-1.8	1.7	1.6
$9/2 - [514] \rightarrow 7/2 + [404]$ b,d)	20	10	3
$7/2 - [514] \rightarrow 7/2 + [404]$ c,d)	-3.5	5.6	4.6
$7/2 - [523] \rightarrow 7/2 + [404]$ c,d)	-0.5	0.9	0.7
$9/2 - [514] \rightarrow 9/2 + [404]$ c,d)	0	4.8	3.4

a) The experimentally determined quantities have been corrected for the small contribution due to the higher order terms in accordance

with Eq. (26).

b) Transitions between dominant components of the wave function.

c) Transitions that involve an admixture in the wave function.

d) The reduction factor due to pairing correlations has not been included.

The best known mechanism for introducing K impurities into the wave functions is the Coriolis interaction[21,51],

$$V = -\frac{1}{\theta}(\vec{I}\cdot\vec{J}). \qquad (33)$$

θ is the moment of inertia about an axis perpendicular to the symmetry axis; $\vec{I}$ and $\vec{J}$ are the total and intrinsic angular momentum operators. Such an interaction connects nuclear states with the same I and π and for which the K values differ by one. Three rotational bands which can cause K impurities in either the initial or final state wave functions are shown in Table VI. The amplitudes of the admixed components of the wave functions were computed using perturbation theory assuming the states are 1 - 2 MeV away. The contributions to the gamma-ray reduced matrix element due to these impurities are given in the table.

All three admixtures give comparable contributions to the transition rates. Certainly, wave functions including all these admixtures can be made to explain the three experimental transition rates if the amplitudes of the admixtures are allowed to vary somewhat. It is clear because of the large disagreement for the 396 keV transition that the contributions from the dominant K_i = 9/2- and

K_f = 7/2+ bands must be reduced by at least an order of magnitude. A reduction of this amount is possible because these matrix elements are uncertain due to both the pairing correlations and, more importantly, the cancellation which has occurred in their computation. Estimation of the admixed contributions are much more reliable since the Coriolis matrix elements are allowed for all the admixtures and the E1 matrix elements are allowed for two of the possible admixtures.

We note that the contributions from the K_i = 7/2- admixtures are indeed very close to explaining the experimental branching ratios. These contributions are also of the right order of magnitude if a factor of $\sim \frac{1}{2}$ due to pairing correlations is used. A reduction factor of this approximate size has been obtained in calculations by Vergnes and Rasmussen[47].

The presence of K impurities due to the Coriolis interaction certainly leads to a qualitative understanding of the E1 transition rates. Any quantitative analysis is necessarily limited by calculational uncertainties. Admixtures in the wave functions of the magnitude considered here have no effect on the earlier estimates of the penetration parameters.

Hf^{177}

The decay scheme of $Lu^{177} \rightarrow Hf^{177}$ is shown in Fig. 12. Although Hf^{177} is an odd neutron nucleus it has a decay scheme similar to Lu^{175}. The 321 keV transition showed large anomalies whereas the 208 and 72 keV transition showed only very small anomalies.

The L subshell spectra for the 321, 208, and 72 keV transi-

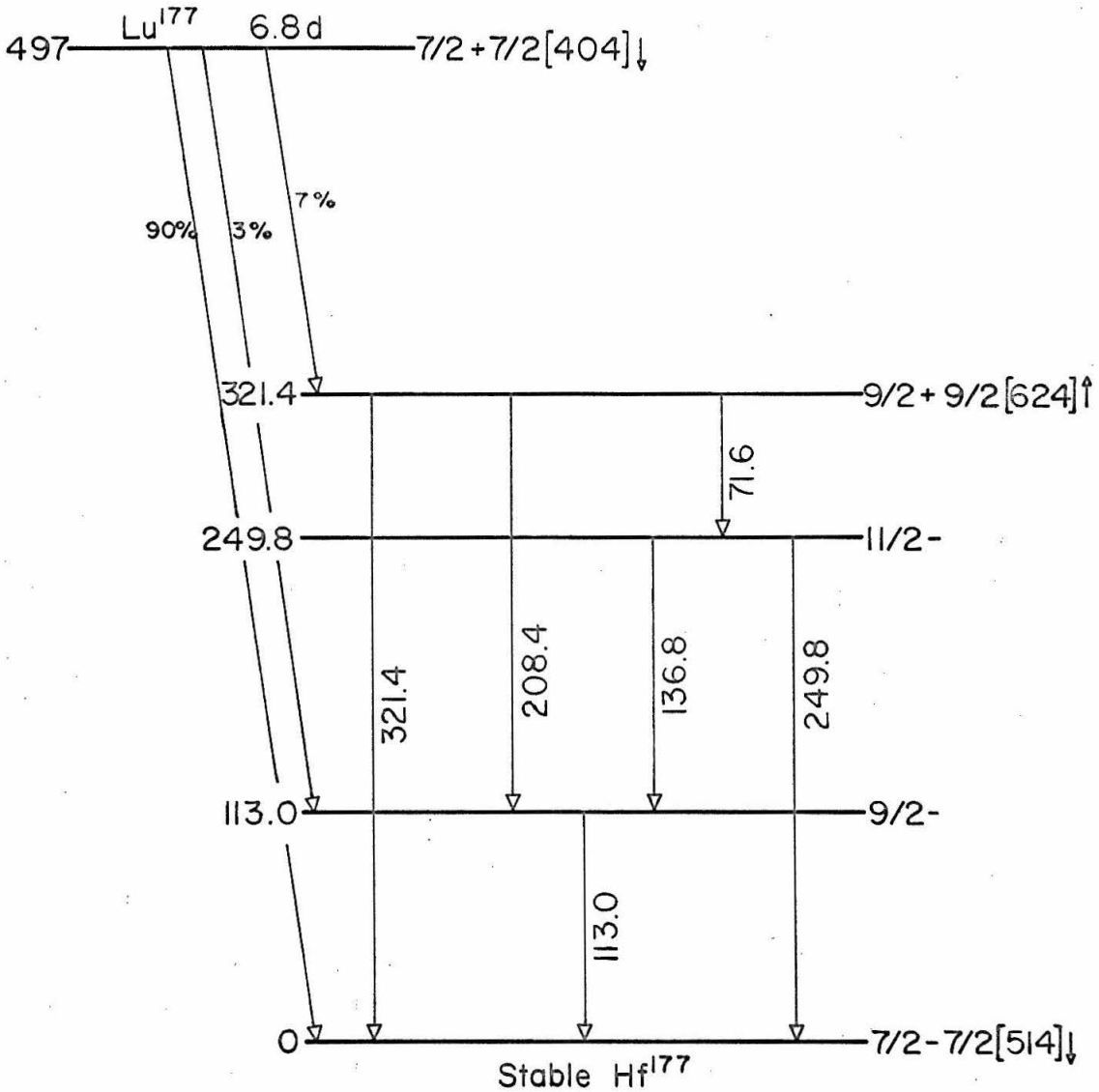

Figure 12

The decay scheme of $Lu^{177} \rightarrow Hf^{177}$. The levels are labeled by the quantum numbers $I\pi K[Nn\Lambda]_{\Sigma}$. The excitation and transition energies are expressed in keV.

tions are shown in Figs. 13, 14, and 15. The experimental difficulty in detecting the 321 keV L_{III} is apparent when the measured intensity of 12×10^3 counts (see Fig. 13) is compared with the subtracted background of 17×10^6 counts. The presence of an anomaly for the 321 keV transition is apparent from the spectrum showing the L_I although the L_{III} is not yet visible, since if the conversion were normal the L_{III} would be slightly larger than the line at the far right of the spectrum due to the 155 day activity. The spectrum of the 72 keV transition also shows the presence of a line from the 155 day decay. The absolute and relative conversion intensities determined from these measurements are given in Table VII. The gamma-ray intensities taken from the work of Alexander, Boehm, and Kankeleit are also included in this table.

Fig. 16 shows $\lambda(j \cdot r)$ as a function of $\lambda(j \cdot \nabla)$ for the 321 keV transition. In spite of the rather large experimental errors, $\lambda(j \cdot r)$ was determined to be -1400 ± 200. The lower part of Fig. 16 shows $\lambda(j \cdot r)$ as a function of δ^2 and indicates that $\delta^2 \lesssim 0.05$. Our experimentally determined α_K and K/L_{III} ratio requires $\delta^2 < 0.02$. As in Lu^{175} the value of $\lambda(j \cdot r)$ is nearly independent of such small M2 admixtures.

The 208 and 72 keV transitions were analyzed with $\lambda(j \cdot \nabla) = 0$ since the introduction of an additional parameter for such small anomalies only complicates the analysis. The values of $\lambda(j \cdot r)$ determined from the various measurements made on these two transitions are shown in Fig. 17. The four values of $\lambda(j \cdot r)$ for the 72

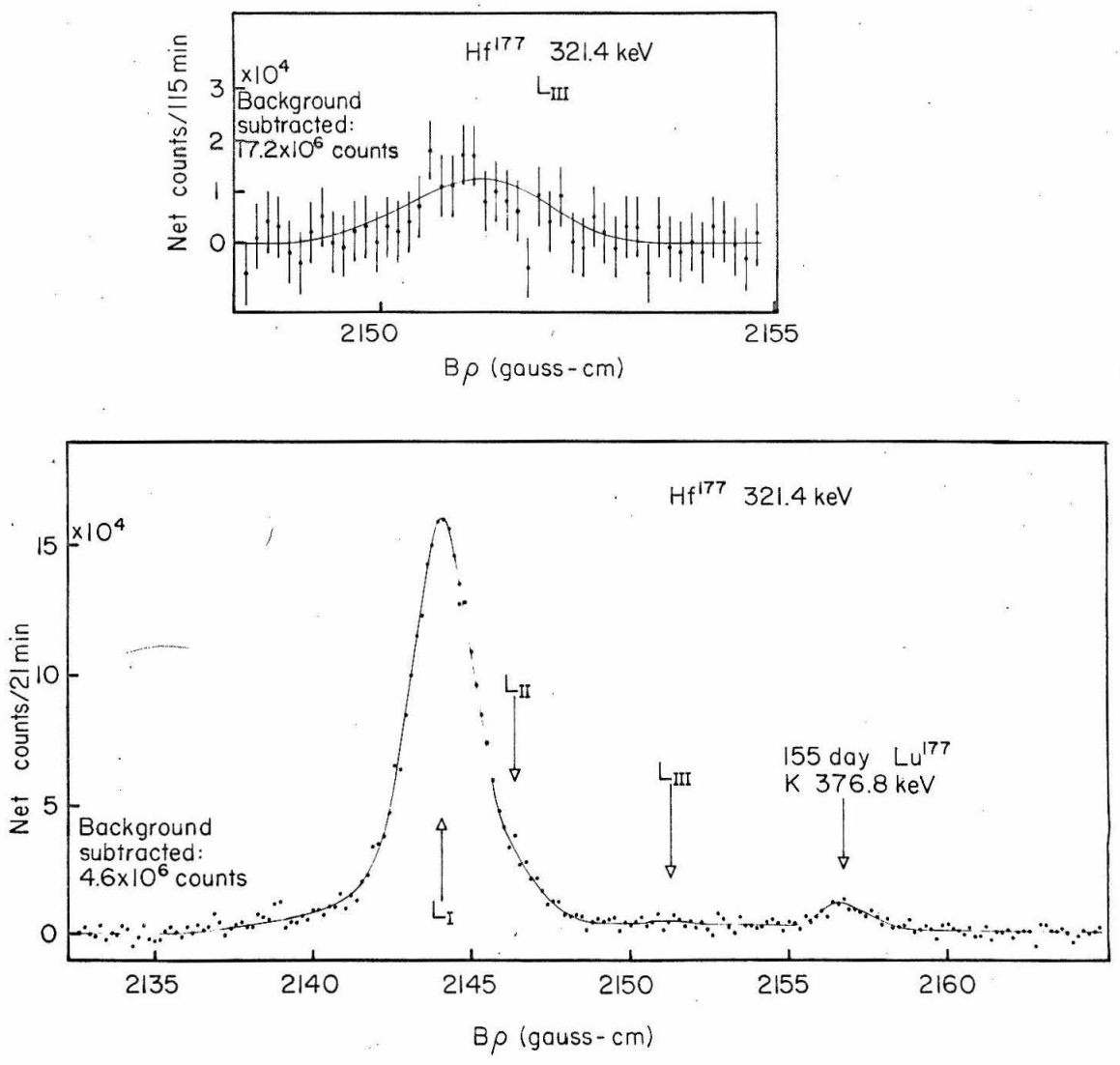

Figure 13.

The L subshell conversion spectrum of the 321 keV transition in Hf^{177} measured at 0.11% momentum resolution with the $\sqrt{2}$ π spectrometer. The L_{III} line is not visible in the lower spectrum which has had a background of approximately 4.6×10^6 counts subtracted from it. The upper plot shows the L_{III} line after a background of approximately 17.2×10^6 counts was subtracted.

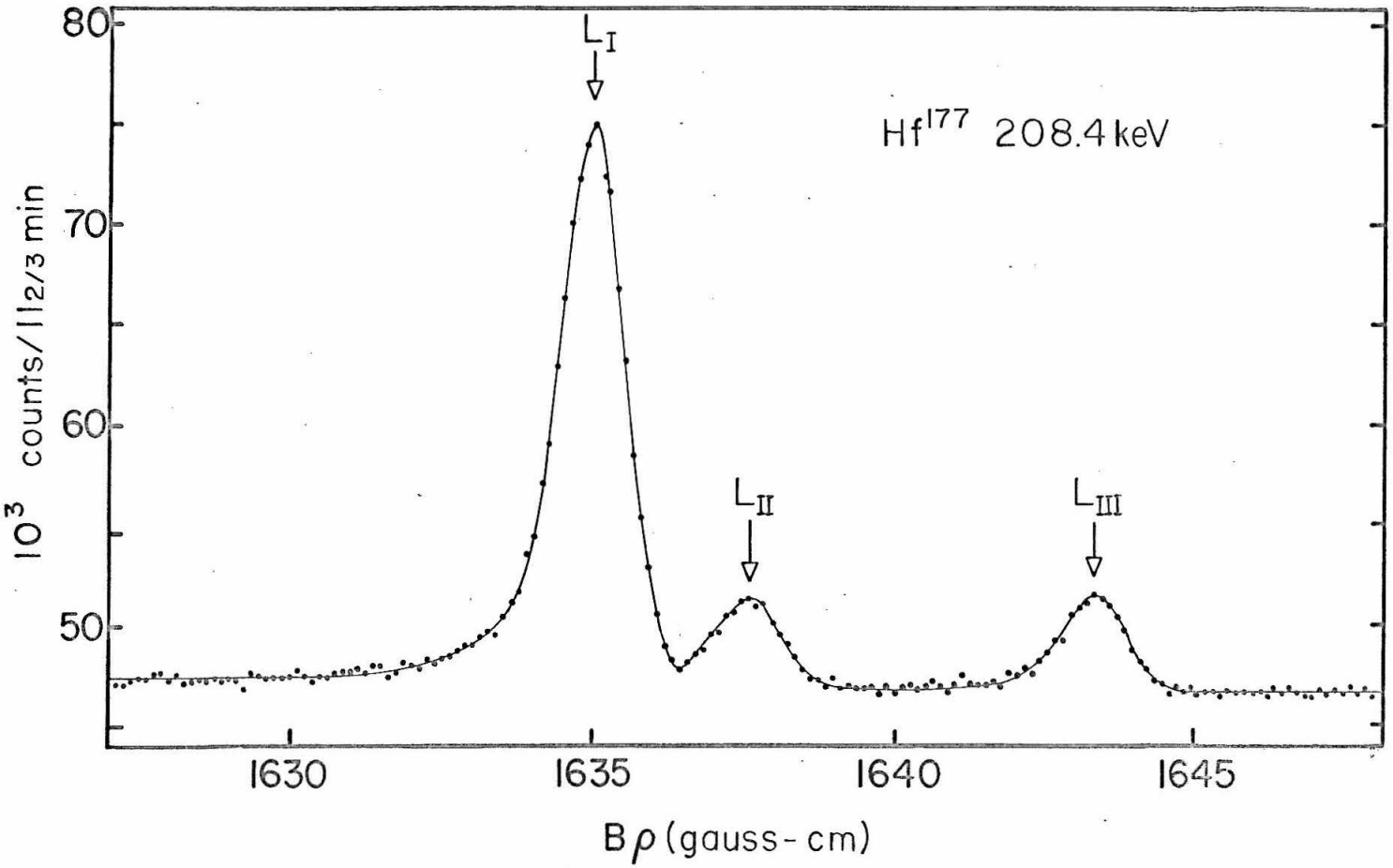

Figure 14

The L subshell conversion spectrum of the 208 keV transition in Hf^{177} measured at 0.07% momentum resolution with the $\sqrt{2}$ π spectrometer.

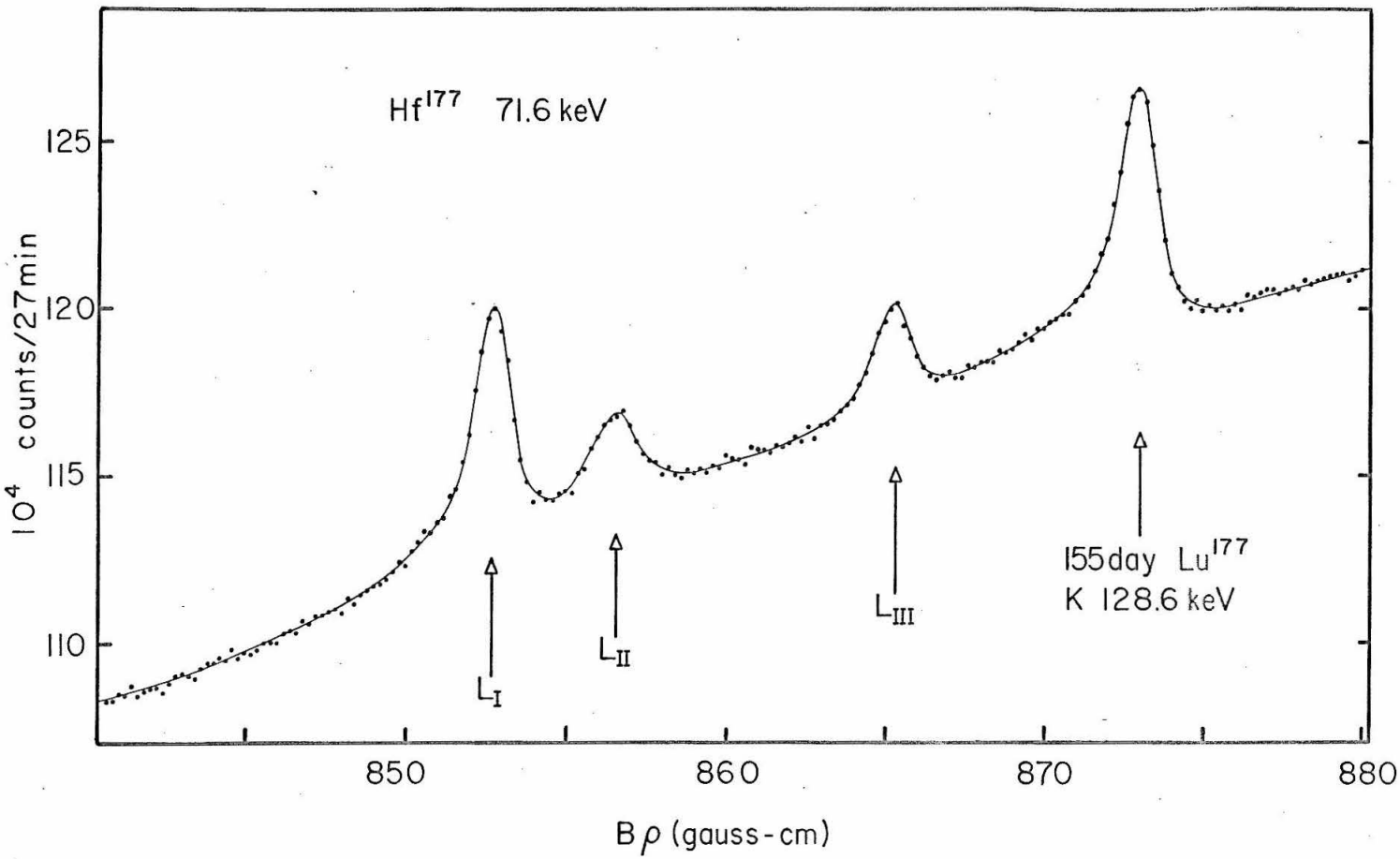

Figure 15

The L subshell conversion spectrum of the 72 keV transition in Hf^{177} measured at 0.17% momentum resolution with the $\sqrt{2}$ π spectrometer. At the right of the spectrum, a line is present from the decay of the 155 day isomeric level in Lu^{177}.

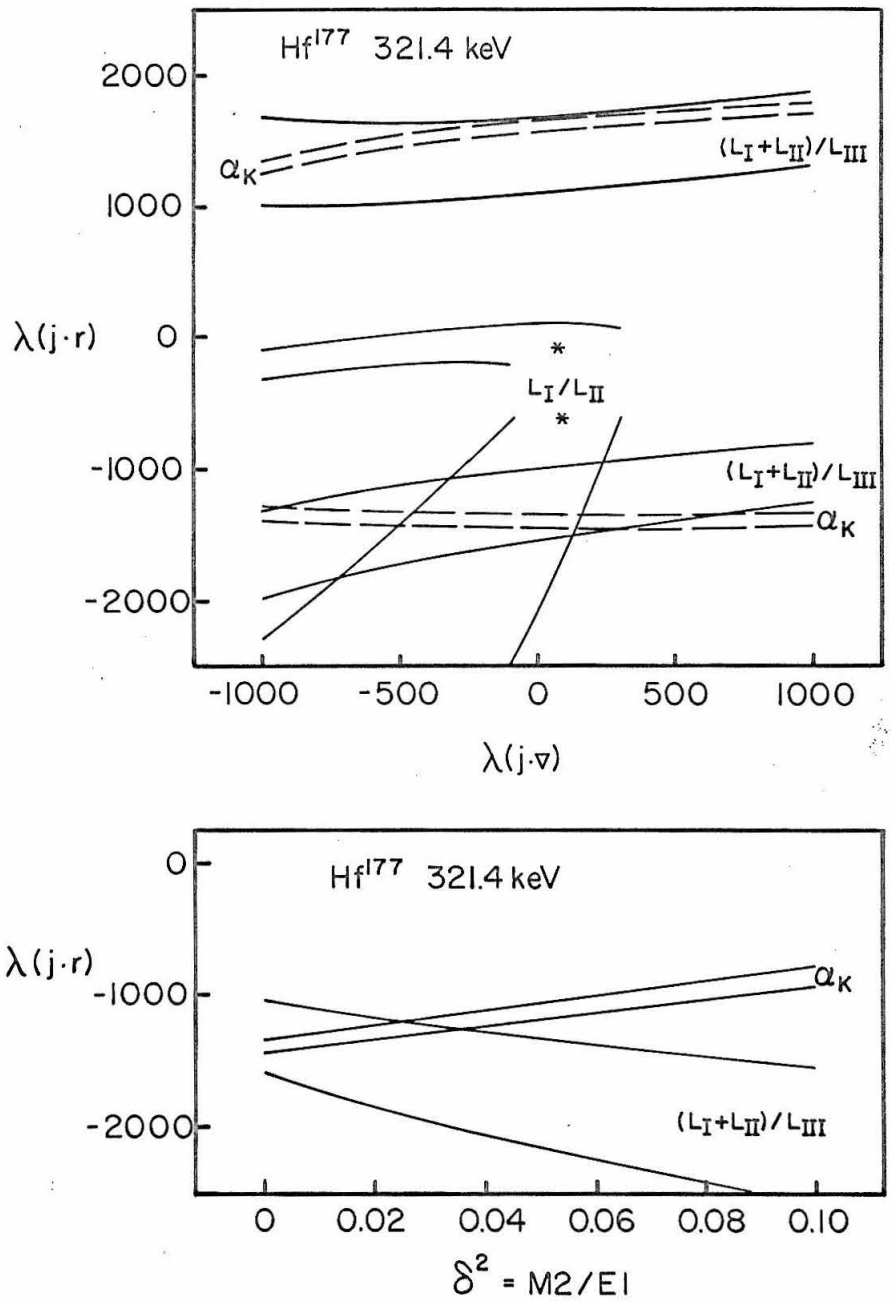

Figure 16

The upper graph shows $\lambda(j\cdot r)$ as a function of $\lambda(j\cdot\nabla)$ for the 321 keV transition in Hf^{177} as determined from the various measurements. For a given measurement (e.g., α_K) the values of $\lambda(j\cdot r)$ and $\lambda(j\cdot\nabla)$ which explain that measurement are contained within a band, the edges of the band representing the limits of experimental error. No. M2 admixture was assumed and the asterisk indicates where $\lambda(j\cdot r)$ becomes complex. The lower graph shows the variation of $\lambda(j\cdot r)$ with $\delta^2 = M2/E1$ for $\lambda(j\cdot\nabla) = 0$.

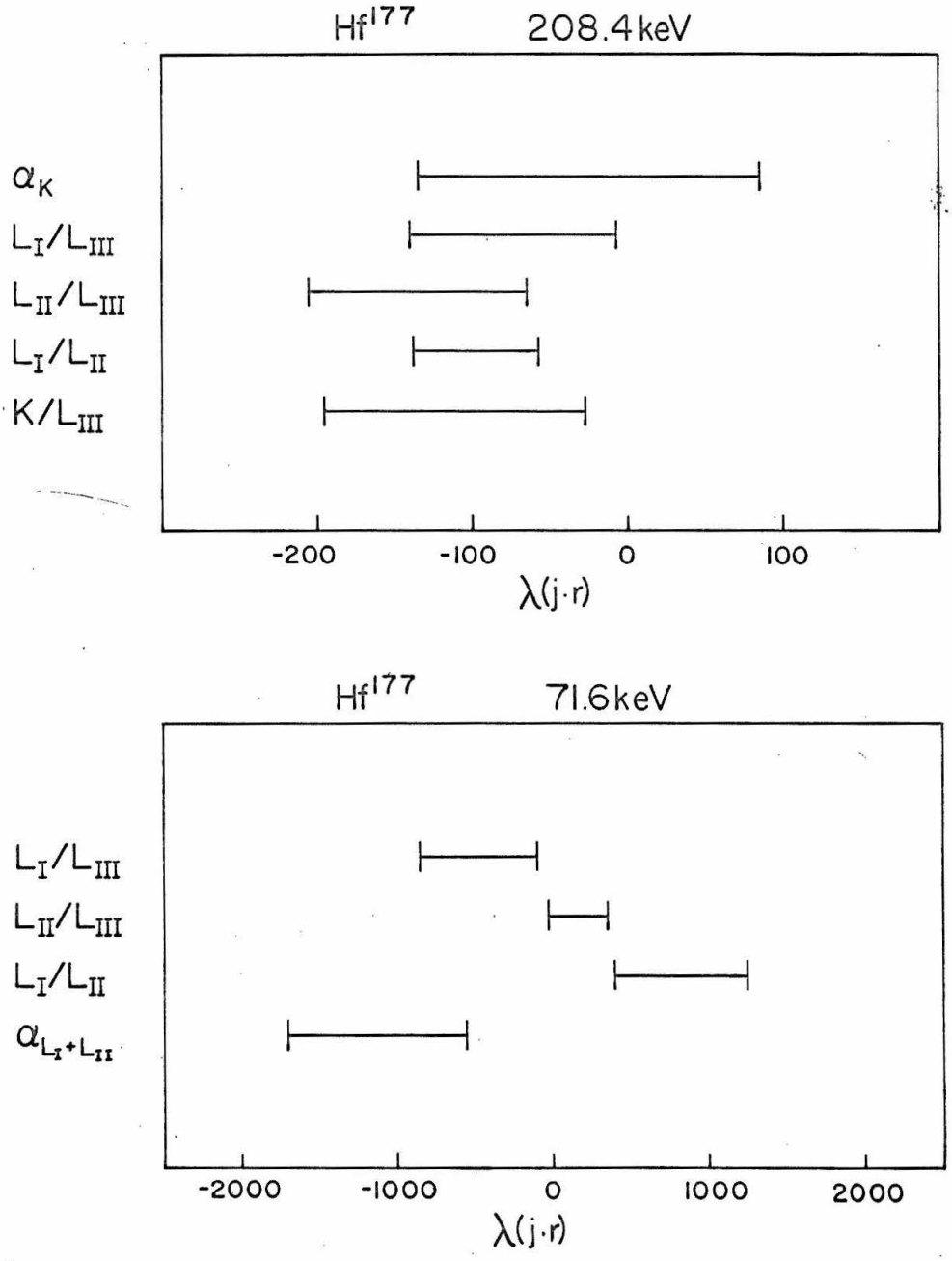

Figure 17

$\lambda(j \cdot r)$ determined from the various measurements for the 208 keV transition (top) and the 72 keV transition (bottom) in Hf^{177}. The error bars represent the experimental errors. In this analysis it was assumed that $\lambda(j \cdot \nabla) = 0$ and that there is no M2 admixture.

TABLE VII

EXPERIMENTAL CONVERSION AND GAMMA-RAY INTENSITIES IN Hf^{177}

Energy (keV)	Gamma-Ray (Relative Units) a)	α_K b)	L_I/L_{II} b)	L_I/L_{III} b)	L_{II}/L_{III} b)
321.4	3.4 ± 0.1	0.084 ± 0.004 (0.0153)	8.5 ± 2.0 (7.7)	$(L_I+L_{II})/L_{III}$ = 60 + 20 (9.2)	
208.4	171 ± 8	0.045 ± 0.002 (0.0445)	6.3 ± 0.2 (5.7)	5.9 + 0.2 (5.7)	0.93 ± 0.03 (0.99)
71.6	2.4 ± 0.1		2.45 ± 0.20 (2.6)	2.55 ± 0.30 (2.2)	1.05 ± 0.15 (0.83)
			$\alpha_{L_I + L_{II}}$ = 0.13 ± 0.02 (0.098)		

a) The gamma-ray intensities are taken from Ref. 26.

b) The theoretical values in parentheses were obtained from the calculations described in Ref. 38.

keV transition are not in complete agreement, although it should be remembered that the limits of $\lambda(j\cdot r)$ for each measurement correspond to the probable errors in that measurement. A weighted average of the four results gives $\lambda(j\cdot r) = 50 \pm 600$ which we rewrite as $|\lambda(j\cdot r)| < 650$. The agreement between the four measurements is improved only slightly when a non-zero $\lambda(j\cdot\nabla)$ is introduced.

The final experimentally determined values of $\lambda(j\cdot r)$ for the three transitions in Hf^{177} are given in Table VIII. The theoretical estimates for the various contributions to $\lambda(j\cdot r)$ for the 321 keV

transition are given in the upper portion of the table. The total theoretical estimate of 2100 compares favorably with the experimental determination of - 1400, in view of the uncertainties mentioned in the discussion of Lu^{175}. The experimental λ's (column 3) are compared with the branching predictions of the rotational model (column 4) in the lower portion of the table. As in the case of Lu^{175} the good agreement demonstrates the usefulness of the model for branching predictions for allowed matrix elements. A calculation of $\lambda(j\cdot\nabla)$ gives 0.2 which is many times less than the experimental limit $|\lambda(j\cdot\nabla)| < 400$ for the 321 keV transition; these numbers are not shown in the table.

TABLE VIII

EXPERIMENTAL AND THEORETICAL PENETRATION PARAMETERS FOR Hf^{177} a)

Energy (keV)	$\lambda(j\cdot r)$ (exp)	$\lambda(j\cdot r)$ (theo)				
		Spin		Convect		Total
		λ_1	λ_2	λ_1	λ_2	
321.4	-1400 ± 200	2500	2500	-60	20	2100

Energy (keV)	$\lambda(j\cdot r)$ (exp)	$\frac{\lambda(E)}{\lvert\lambda(321)\rvert}\left(\frac{E}{321}\right)$	R	Sign of M_γ
321.4	-1400 ± 200	-1.0	1.0	-
208.4	-90 ± 40	-0.05 ± 0.02	0.03	-
71.6	$\lvert\lambda\rvert < 650$	$\lvert\lambda\rvert < 0.10$	0.02	?

a) Explanations for the entries in the table are identical with those

of Table V if 321 keV is read in place of 396 keV.

The effect of band mixing on the E1 gamma-ray transition probabilities has been discussed briefly by Vergnes and Rasmussen[47]. They have shown that the simple assumption of a Coriolis admixture of a K = 7/2+ component into the predominant K_i = 9/2+ band affords a semi-qualitative explanation of nine E1 transition probabilities as determined by Alexander, Boehm, and Kankeleit[26] from the decay of 155 day Lu^{177m}. The decay of Lu^{177m} populates high spin states in the K_i = 9/2+ and K_f = 7/2- bands in Hf^{177} which are not populated in the decay of the seven day Lu^{177}. As a result nine interband E1 transitions are observed in the decay of Lu^{177m} instead of just the three observed in the decay of Lu^{177}.

We have calculated that the admixture of the K = 7/2+[624] band in the K_i = 9/2+ band is $\sim \frac{1}{2}$ %. Although this impurity has allowed E1 matrix elements with the K_f = 7/2- ground state band, the resultant contribution to the gamma-ray matrix elements is about a factor of 5 - 10 smaller than the magnitude required by the analysis of Vergnes and Rasmussen. Unexpected cancellation has occurred in the calculation of the Coriolis matrix element and therefore we believe the above estimate is unreliable. There are no other K = 7/2+ bands that are expected to mix strongly. The reduction factor due to pairing correlations is expected to be small so that too is uncertain. We have shown that the phases of the 208 and 321 keV gamma-ray matrix elements determined in our experiments are consistent with the analysis of Vergnes.

As in the case of Lu^{175} the E1 transition probabilities in

Hf^{177} can qualitatively be understood in terms of wave function impurities due to the Coriolis interaction. However, little seems to be learned by quantitative calculations.

Tm^{169} and Gd^{155}

The initial and final state assignments for the transition investigated in each nucleus is shown in Table IX. These two cases are interesting because all first order contributions to $\lambda(j \cdot r)$ are hindered. It is the second order terms which may be most important since the second order contribution is allowed for the spin current in Tm^{169} and for the convection current in Gd^{155}. Only very small anomalies were observed for both transitions. The L subshell ratios are given in Table X along with the theoretical values in parentheses.

TABLE IX

INITIAL AND FINAL STATES FOR THE Tm^{169} 63.1 keV AND Gd^{155} 86.5 keV TRANSITIONS

Nucleus Energy(keV)	Initial State a)	Final State a)
Tm^{169} 63.1	7/2 - 7/2[523]↑	7/2 + 7/2[404]↓
Gd^{155} 86.5	3/2 + 3/2[651]↑	3/2 + 3/2[521]↑

a) The state assignments are represented by the usual quantum numbers $I\pi K[Nn\Lambda]\Sigma$.

TABLE X

EXPERIMENTAL CONVERSION INTENSITIES

IN Tm^{169} AND Gd^{155}

Nucleus Energy(keV)	L_I/L_{II} a)	L_I/L_{III} a)	L_{II}/L_{III} a)
Tm^{169} 63.1	2.78 ± 0.05 (2.70)	2.23 ± 0.04 (2.14)	0.80 ± 0.02 (0.79)
Gd^{155} 86.5	4.4 ± 0.2 (4.2)	3.4 ± 0.1 (3.3)	0.77 ± 0.04 (0.79)

a) The theoretical values in parentheses were obtained from the calculations described in Ref. 38.

The solutions of $\lambda(j\cdot r)$ with $\lambda(j\cdot\nabla) = 0$ for each L subshell ratio are shown in Fig. 18. Unfortunately, the anomalies are small and consequently it is more difficult to accurately determine $\lambda(j\cdot r)$. A weighted average of the three measurements gives $\lambda(j\cdot r) = -100 \pm 100$ for the Tm^{169} transition and $\lambda(j\cdot r) = -150 \pm 100$ for the Gd^{155} transition. Neither result conclusively proves the existence of a non-zero λ but the measurements definitely seem to be interpreted best in terms of non-zero λ's.

These experimentally determined λ's are compared with the theoretically calculated λ's in Table XI. In Tm^{169} the second order spin current contribution is the largest as expected but the four contributions tend to cancel leaving only - 70 for the resultant $\lambda(j\cdot r)$. In Gd^{155} the second order convection current contribution,

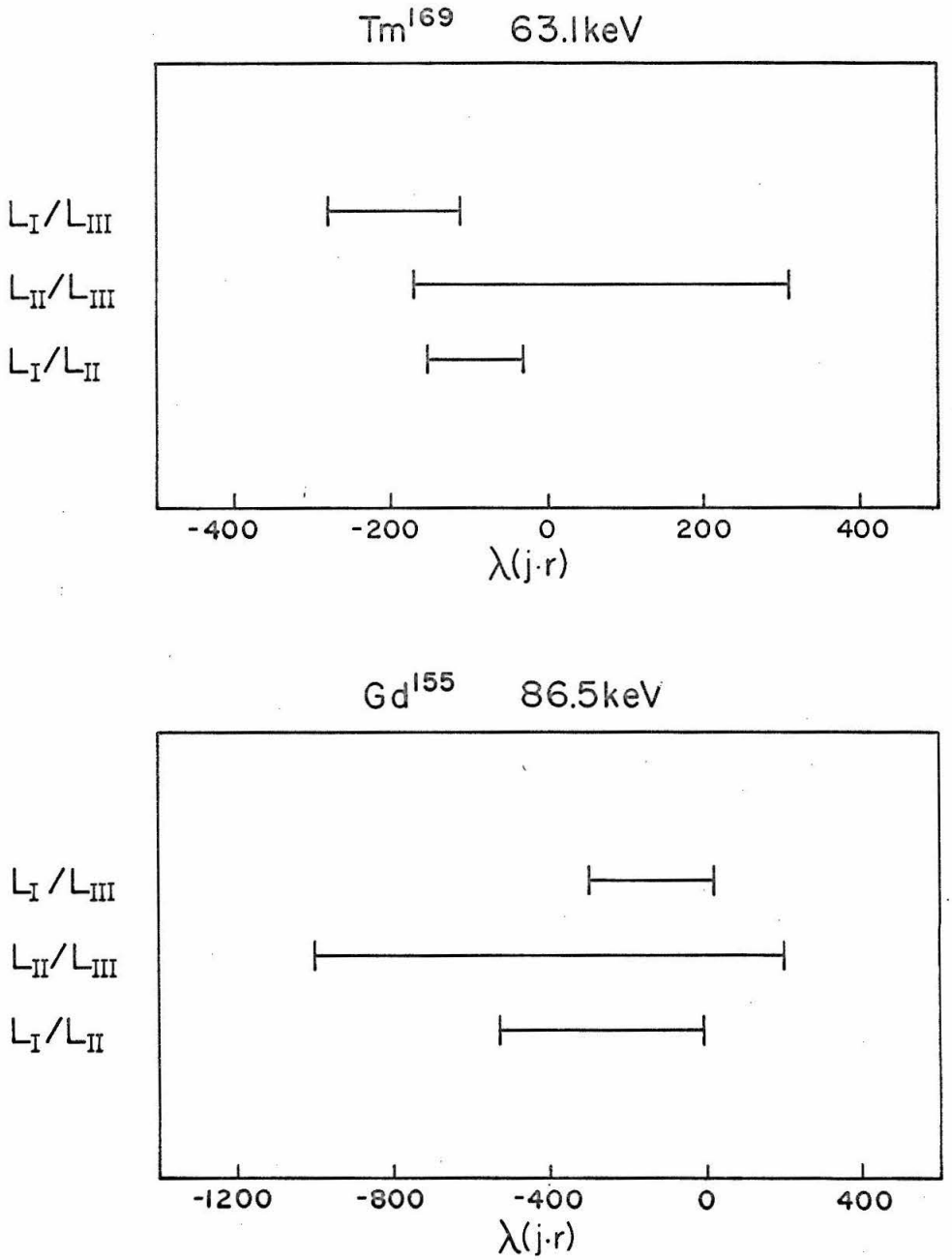

Figure 18

$\lambda(j\cdot r)$ determined from the various measurements for the 63 keV transition in Tm^{169} (top) and the 86 keV transition in Gd^{155} (bottom). The error bars represent the experimental errors. In this analysis it was assumed that $\lambda(j\cdot\nabla) = 0$ and there is no M2 admixture.

which was expected to be largest, was calculated to be only - 20.

TABLE XI

EXPERIMENTAL AND THEORETICAL PENETRATION PARAMETERS FOR Tm^{169} AND Gd^{155}

Nucleus Energy (kev)	$\lambda(j\cdot r)$ (exp)	$\lambda(j\cdot r)$ (theo)				
		Spin a)		Convect b)		Total
		λ_1	λ_2	λ_1	λ_2	
Tm^{169} 63.1	-100 ± 100	40	-400	-200	-200	-70
Gd^{155} 86.5	-150 ± 100	15	60	100	-20	100

a) Calculated using the second term of the second equation in (15).

b) Calculated using the first term of the second equation in (15).

c) Calculated using the second equation of (23) neglecting the terms for $m \geq 3$. Since β_2/β_1 is very close to -7 this sum is just $\lambda_1(j_c\cdot r) + \lambda_1(j_s\cdot r) - (1/7)(\lambda_2(j_c\cdot r) + \lambda_2(j_s\cdot r))$.

This small value can be understood in terms of the following explanation. The initial and final states (see Table IX) are connected by the operator z^3r^2 which is contained in the second order convection current operator $r^2z(\vec{r}\cdot\vec{\nabla} + 3)$ (see Table I). In terms of the asymmetric harmonic oscillator Hamiltonian this operator can be written as:

$$\frac{M}{3} r_\perp^2[z^3, H_z] + \frac{M}{2} z^3[r_\perp^2, H_{r_\perp}] + \text{"other terms"}$$

where the "other terms" cannot connect the initial and final states.

The dominant part of the matrix element of the first and second terms of this operator cancel leaving only terms proportional to the deformation ϵ which is equivalent to the matrix element being asymptotically hindered. In spite of this unexpected cancellation a value of 100 is calculated for the resultant $\lambda(j \cdot r)$. There is good agreement between the experimentally determined and the calculated values of $\lambda(j \cdot r)$ for both cases.

Unfortunately, the agreement may be fortuitous since both the experimental and theoretical λ's have limited reliability. The theoretical estimates are somewhat uncertain because the contributions are comparable and tend to cancel. Furthermore, most of the contributions are hindered and the result of cancellation, although the cancellation is not as strong as in the calculation of the gamma-ray matrix elements. The experimental λ's are uncertain because the observed anomalies are small and consequently the accuracy of the theoretical conversion coefficients is an important factor. These inaccuracies are generally accepted to be a few percent. Fortunately, much of the inaccuracy tends to cancel out in relative measurements such as the L subshell measurements made in the present investigations. This is perhaps why for small anomalies L subshell measurements tend to give consistent results whereas the absolute conversion measurements tend to give conflicting results. In order to complete the analysis of the experiments it was necessary in these cases to neglect the absolute conversion measurements. It is known[38] that E2 L subshell conversion exhibits small anomalies which can not be attributed to penetration effects; the origin of such anomalies is presently unknown.

Such effects are possible in E1 conversion. The accuracy of the theoretical conversion coefficients is too limited to accurately be able to determine the magnitude of small penetration anomalies. Nevertheless, we note that the observed anomalies with respect to the present theoretical conversion coefficients can be interpreted rather well in terms of nuclear structure effects.

W^{182}

W^{182}, having an even number of both protons and neutrons, cannot be described in terms of single particle excitations. The lowest intrinsic excitations will be either collective excitations or two particle excitations. The two transitions investigated are transitions from two rotational levels of a two particle state to a collective vibrational state. A partial decay scheme of $Ta^{182} \rightarrow W^{182}$ is shown in Fig. 19, [514↑ - 402↑] being the proton-proton two quasi-particle designation according to Soloviev[52]. A proton with $\Omega = \Lambda + \Sigma = 9/2$ and a proton with $\Omega = 5/2$ are coupled to give a $K = 2$ state. The collective state is a γ-vibrational state representing small oscillations such that the deformed nucleus loses its axial symmetry.

The L subshell spectra for the 67.7 and the 152.4 keV transitions are shown in Figs. 20 and 21. Figure 22 shows the complex spectrum associated with the 152 keV α_K measurement. The close-lying 84 keV M and N lines were almost completely resolved except for the M_{IV} and M_V lines which are expected to contribute less than 1% to the 152 keV K intensity. The 152 keV L_{III} line was compared with a pure E2 line (229 keV K) present in the spectrum and this comparison

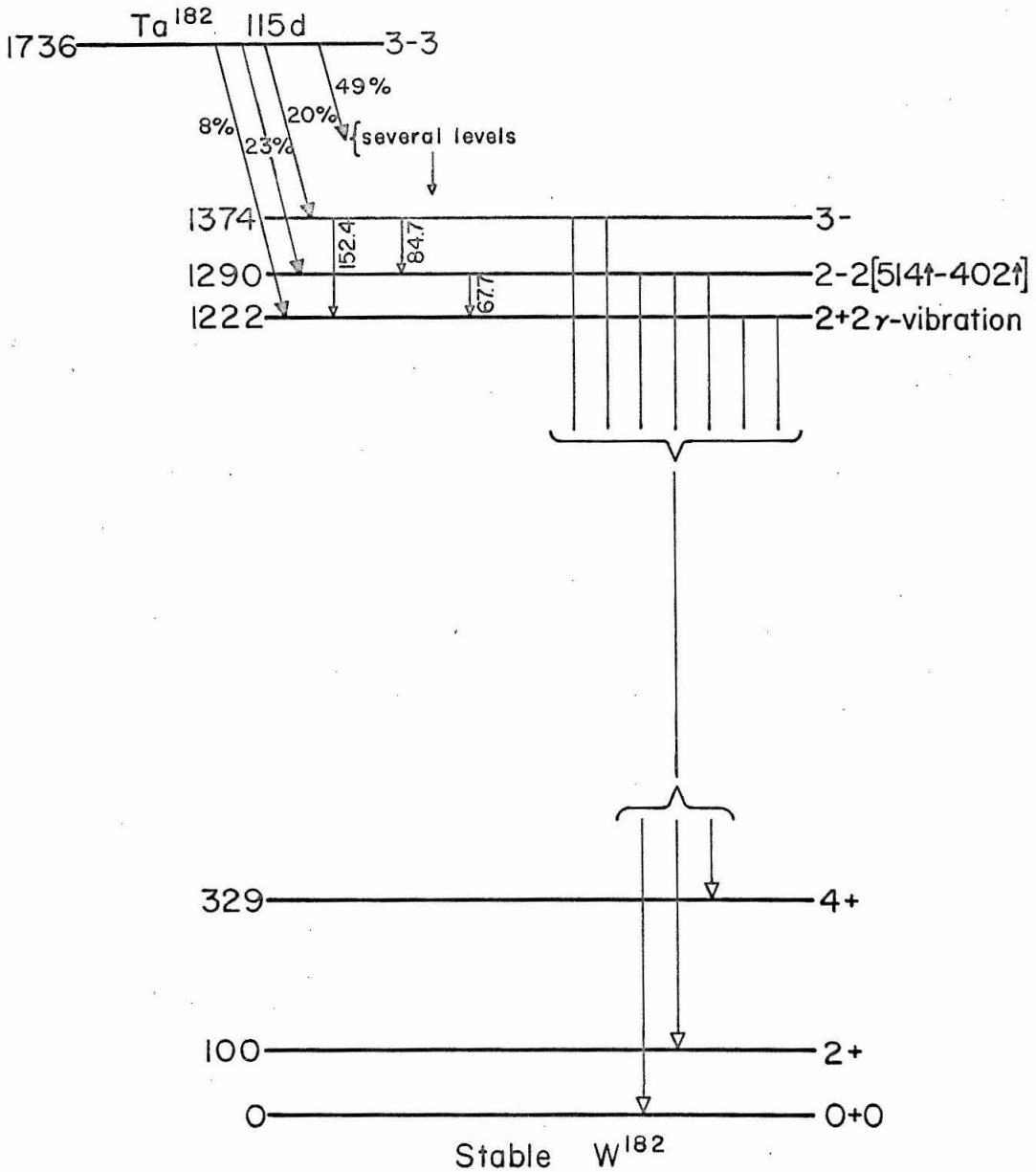

Figure 19

A partial decay scheme of $Ta^{182} \rightarrow W^{182}$. The excitation and transition energies are expressed in keV. The states are labeled by the quantum numbers IπK.

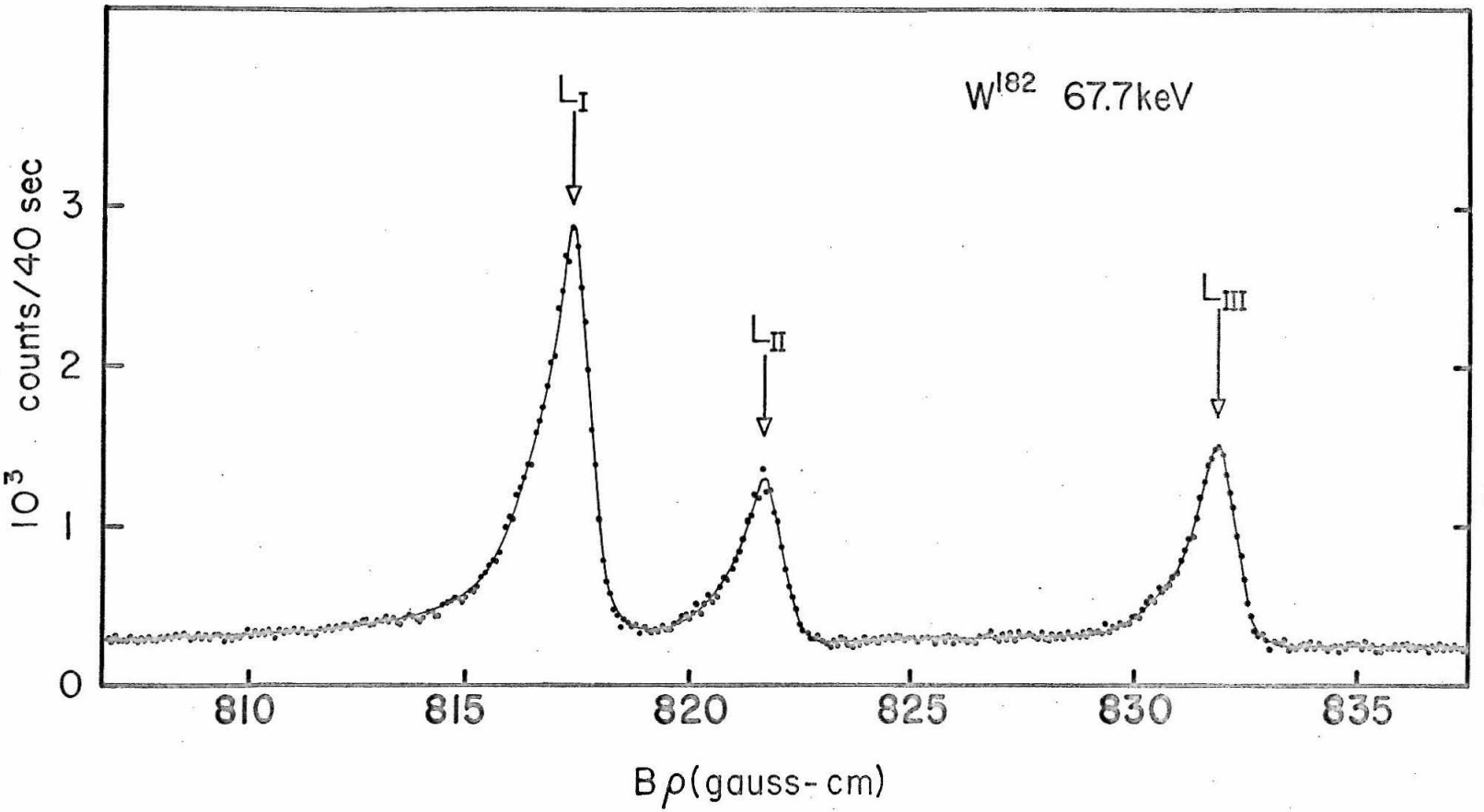

Figure 20

The L subshell conversion spectrum of the 67 keV transition in W^{182} measured at 0.14% momentum resolution with the $\sqrt{2}$ π spectrometer.

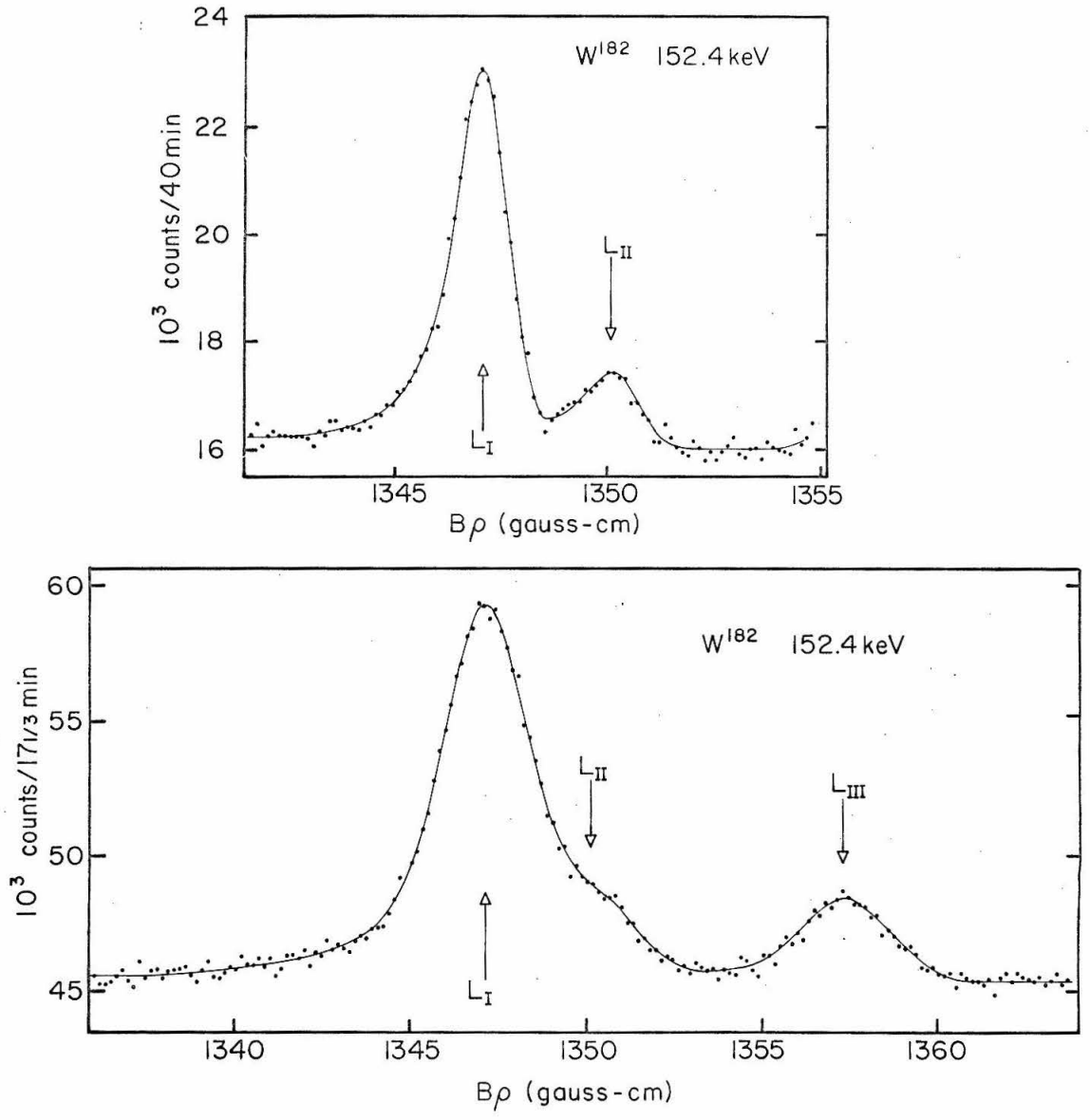

Figure 21

The L subshell conversion spectrum of the 152 keV transition in W^{182} measured with the $\sqrt{2}\,\pi$ spectrometer. The L_I/L_{II} ratio was obtained from the upper spectrum measured at 0.11% momentum resolution. The $(L_I + L_{II})/L_{III}$ ratio was obtained from the lower spectrum measured at 0.22% resolution.

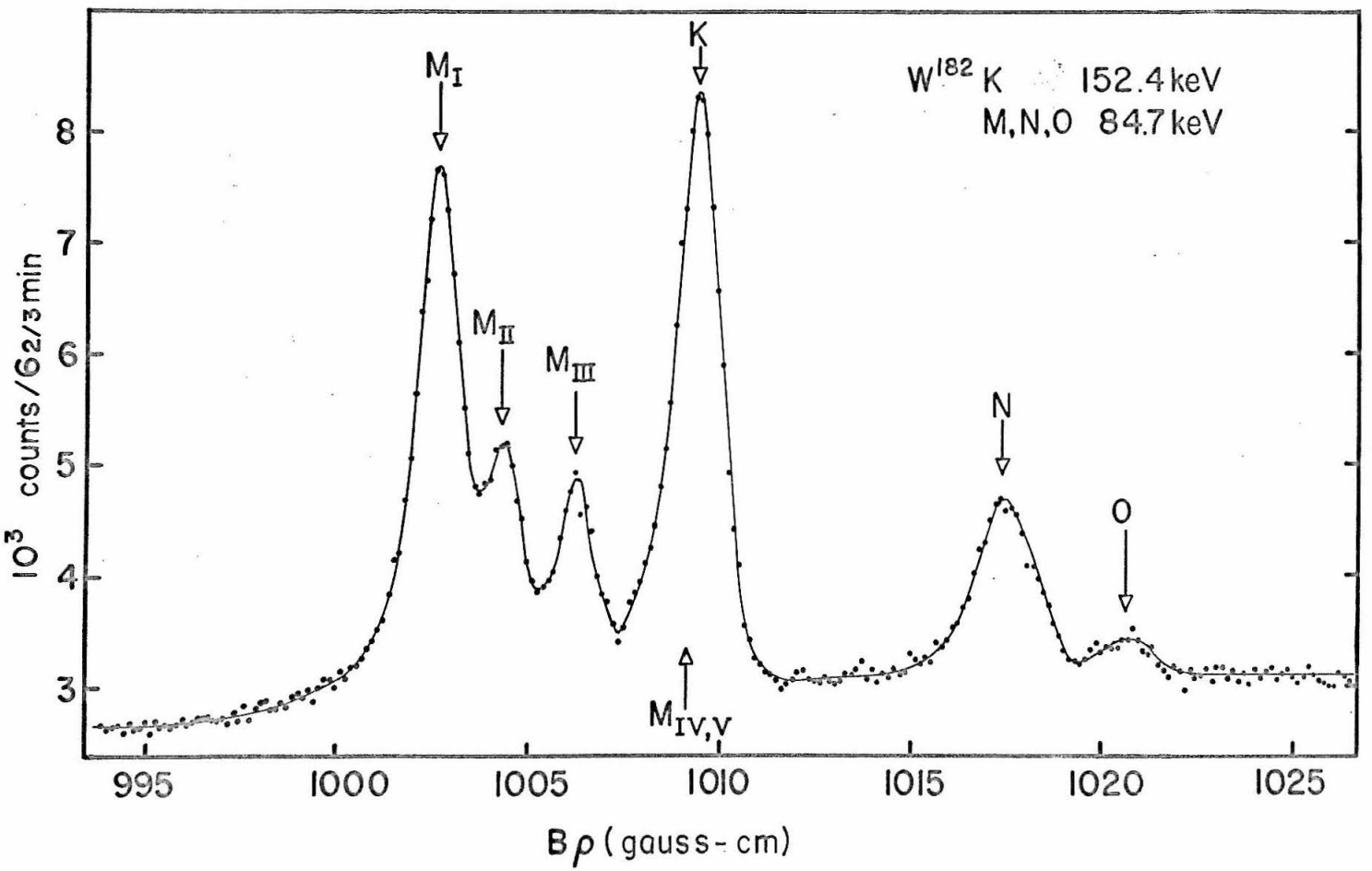

Figure 22

The K shell conversion spectrum of the 152 keV transition in W^{182} measured at 0.14% momentum resolution with the $\sqrt{2}$ π spectrometer. The close lying 84 keV M, N, and O shell lines are shown.

indicated an M2 admixture of less than 0.1%. The experimental conversion intensities are given in Table XII. Again the observed anomalies were very small.

TABLE XII

EXPERIMENTAL CONVERSION

INTENSITIES IN W^{182}

Energy (keV)	α_K a)	L_I/L_{II} a)	L_I/L_{III} a)	L_{II}/L_{III} a)
152.4	0.095 ± 0.005 (0.107)	5.0 ± 0.3 (4.4)	4.75 ± 0.20 (4.1)	0.95 ± 0.06 (0.93)
67.7		2.54 ± 0.12 (2.38)	2.02 ± 0.08 (2.00)	0.80 ±0.02 (0.84)

a) The theoretical values in parentheses were obtained from the calculations described in Ref. 38.

The values of $\lambda(j\cdot r)$ with $\lambda(j\cdot\nabla) = 0$ corresponding to the individual measurements are shown in Fig. 23. The small anomalies do not give good determinations of $\lambda(j\cdot r)$ but again the results seem to indicate non-zero values of $\lambda(j\cdot r)$. Because of the complex spectrum for the 152 keV K line and also because of the previously mentioned difficulties with absolute conversion measurements the α_K measurement was disregarded in obtaining the weighted average of $\lambda(j\cdot r)$ for the 152 keV transition. The final values of $\lambda(j\cdot r)$ are - 100 ± 100 for the 67 keV transition and - 160 ± 80 for the 152 keV transition. These are given in Table XIII. Also given in this table are the branching predictions of the rotational model. Although the accuracy

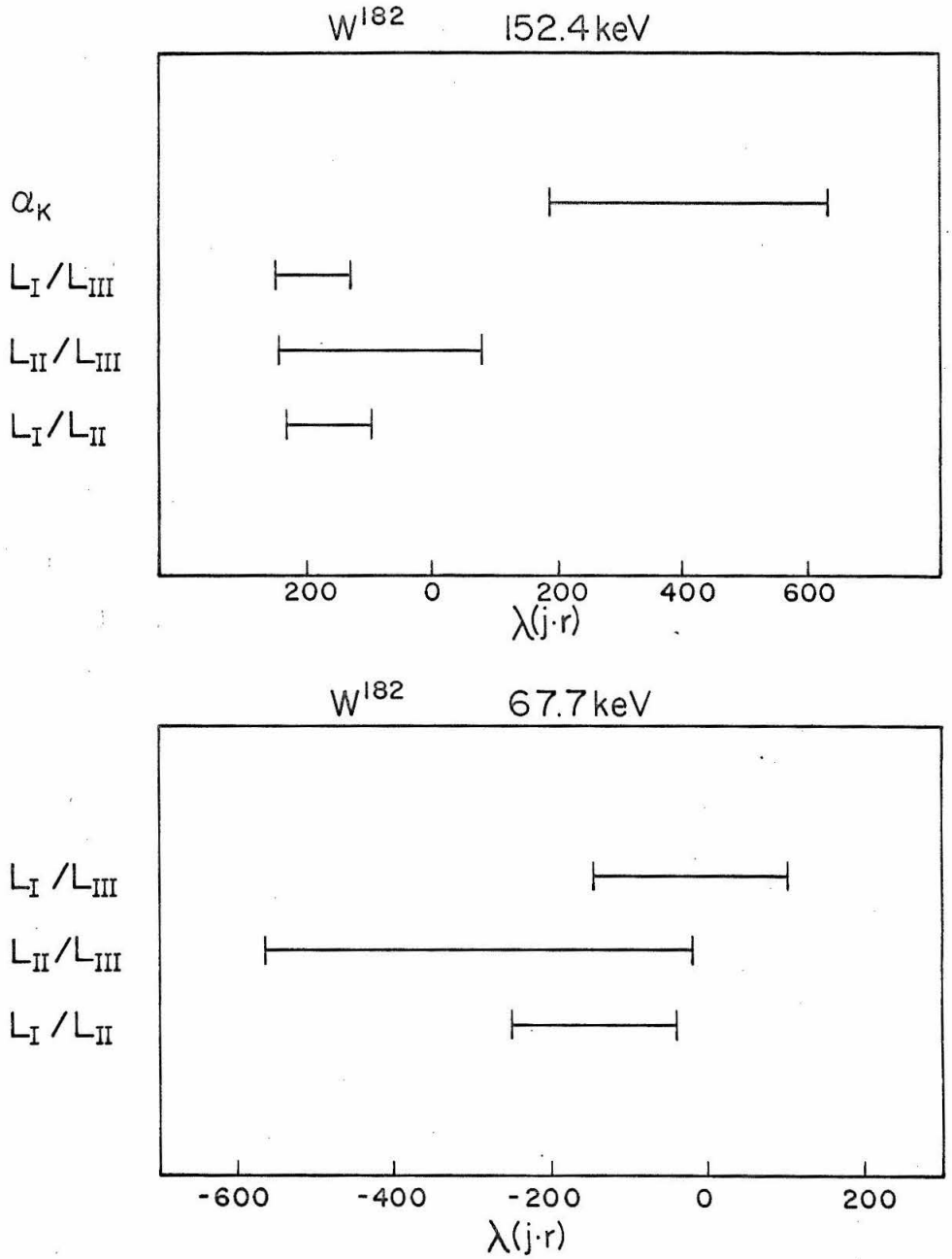

Figure 23

$\lambda(j\cdot r)$ determined from the various measurements for the 152 keV transition (top) and the 67 keV transition (botton) in W^{182}. The error bars represent the experimental errors. In this analysis it was assumed that $\lambda(j\cdot\nabla) = 0$ and there there is no M2 admixture.

of the experimental λ's is not good, a comparison seems to indicate compliance with the model predictions.

TABLE XIII

EXPERIMENTAL AND THEORETICAL PENETRATION PARAMETERS FOR W^{182}

Energy (keV)	$\lambda(j\cdot r)$ (exp)	$\frac{\lambda(E)}{\lambda(152)}\left(\frac{E}{152}\right)_{a)}$	R b)
152.4	-160 ± 80	1.0	1.0
67.7	-100 ± 100	0.3 ± 0.3	0.22

a) The experimentally determined $\lambda(j\cdot r)$ normalized to 1.0 for the 152 keV transition. The λ's are multiplied by the transition energy to remove all energy dependence.

b) Calculated from Eq. (28) where the prime refers to the 152 keV transition.

Due to the complex structure of the collective state we are unable to make any predictions for the magnitude of the above λ's. Bes et al.[53] have investigated the structure of the γ-vibrational states within the framework of the superfluid nuclear model*). The wave function of a collective state appears as the superposition of the

---

*) In this model the interaction Hamiltonian between nucleons is written as[43,54]

$$H = H_{av} + H_{pair} + H_{coll}.$$

H_{av} is the average nuclear field (usually the deformed single particle orbits of Nilsson); H_{pair} and H_{coll} are the pairing

(continued on following page)

wave functions of two quasiparticle states. Bes gives the amplitudes of the various components of the γ-vibrational state in W^{182} for components which occur with amplitudes larger than 0.07. According to Bes all the components of the γ-vibrational state which can be connected with the two quasiparticle state [514↓ - 402↑] by a single particle operator (with a change of parity and $\Delta K = 0$) have amplitude ≤ 0.07. This qualitatively explains the retardation of the E1 gamma-ray transition probability since only three components have allowed matrix elements. Moreover, the penetration contributions will also be reduced if the various components of the γ-vibrational state do not give matrix elements which all have the same phase. In view of this, large λ's would not be likely.

(continuation of the footnote from previous page)

and long range residual interactions. The part of H_{coll} which directly affects the energy of the γ-vibrational states is of the form $gQ_{22}Q_{2-2}$ where Q_{22} is the quadrupole moment operator and g is the strength of the interaction.

CHAPTER VII

SUMMARY AND CONCLUSIONS

There are two distinctly different types of penetration matrix elements which contribute to E1 internal conversion, the $j \cdot r$ type and the $j \cdot \nabla$ type. From dimensional arguments one expects $|\lambda(j \cdot r)| \gg |\lambda(j \cdot \nabla)|$ which is consistent with our lack of evidence that $\lambda(j \cdot \nabla)$ is important in the interpretation of the experiments. In fact, the experiments can adequately be analyzed in terms of only $\lambda(j \cdot r)$.

For large anomalies the L subshell spectra show that the L_I and L_{II} intensities are stronger than expected while the L_{III} intensity is very close to normal. α_K is also larger than expected for normal conversion. This pattern also implies that the $j \cdot r$ type of matrix elements is dominant since the $j \cdot \nabla$ type should affect all three L subshells in a comparable eay. We have seen that for the larger anomalies $\lambda(j \cdot r)$ can be determined rather well from the experiments with a knowledge of the electron dependent factors.

For small anomalies there are no systematic patterns in the L subshell spectra. The care required to obtain accurate electron intensities in such cases was discussed. The accuracy and reliability of the values of $\lambda(j \cdot r)$ determined from these experiments is necessarily limited because of the small anomalies and the accuracy with which the electron dependent factors are known.

We have seen that the unified nuclear model predicts the penetration matrix elements fairly well. The gamma-ray matrix elements were taken from experiment since the model does not predict these well.

Within a factor of two the spin current accounts for the penetration parameters in the spin flip transitions in Hf^{177} and Lu^{175}. The predictions for the cases with small anomalies are more uncertain due to cancellation but are, nevertheless, satisfactory. The simple branching rules predicted by the rotational model explain the branching of the penetration matrix elements between two rotational bands quite well.

The theoretical calculations of $\lambda(j \cdot r)$ are somewhat uncertain due to the effects of spin polarization and pairing correlations. An effective value of the nuclear magnetic moment was used to estimate the effects of spin polarization. Pairing correlations are expected to have little effect on the $j \cdot r$ type of penetration matrix element. The $j \cdot \nabla$ matrix elements can be strongly effected by pairing correlations because the $j \cdot \nabla$ types of matrix elements (penetration and gamma-ray) have opposite time reversal properties from the $j \cdot r$ type.

Comparison of the experimentally determined $\lambda(j \cdot r)$ with the model predictions has allowed us to determine the phase of the gamma-ray matrix elements. This additional information has helped in some cases to qualitatively understand the retardation of the gamma-ray matrix elements in terms of the Coriolis interaction. By using the gamma-ray matrix elements in the long wavelength approximation, the contribution of the $j \cdot r$ matrix elements to the gamma-ray transition probability has been neglected. We have seen that for some highly retarded transitions the $j \cdot r$ matrix elements cause a 20% correction to the usual $j \cdot \nabla$ gamma-ray matrix elements.

APPENDIX I

FORM OF THE PENETRATION TERMS

The transition probability for electron emission is taken to be (see Rose[55])

$$N_e = \frac{2\pi}{137} \left| \iint d\tau_n d\tau_e \; (\vec{j}_n \cdot \vec{j}_e - \rho_n \rho_e) \; \frac{e^{ikr'}}{r'} \right|^2 , \qquad (34)$$

where j and ρ are the current and charge densities. The subscripts n and e refer to the nucleus and electron, and $r' = \left| r_n - r_e \right|$. For an electron $j_e = \psi_f^* \alpha \psi_i$, $\rho = \psi_f^* \psi_i$ where α is Dirac's velocity operator and the ψ's are the initial and final electron wave functions.

The scalar part of the retarded interaction can be written

$$\rho_n \rho_e \frac{e^{ikr'}}{r'} = 4\pi ik \sum_{L,M} \left[\rho_n j_L(kr_n) Y^*_{LM}(\hat{r}_n) \right] \left[\rho_e h_L(kr_e) Y_{LM}(\hat{r}_e) \right] , r_n \leq r_e$$

$$= 4\pi ik \sum_{L,M} \left[\rho_n h_L(kr_n) Y^*_{LM}(\hat{r}_n) \right] \left[\rho_e j_L(kr_e) Y_{LM}(\hat{r}_e) \right] , r_n \geq r_e . \qquad (35)$$

In these expressions $j_L(kr)$ and $h_L(kr)$ are the spherical Bessel function and Hankel function of the first kind of order L. Y_{LM} is the usual spherical harmonic. The expansion of the current part of the interaction requires the use of vector spherical harmonics and can be written in the form (36)

$$\vec{j}_n \cdot \vec{j}_e \frac{e^{ikr'}}{r'} = 4\pi ik \sum_{L,M,i} \left[\vec{j}_n(r_n) \cdot \vec{A}^{i*}_{LM}(kr_n) \right] \left[\vec{j}_e(r_e) \cdot \vec{B}^{i}_{LM}(kr_e) \right] , \; r_n \leq r_e ,$$

$$= 4\pi ik \sum_{L,M,i} \left[\vec{j}_n(r_n) \cdot \vec{B}^{i*}_{LM}(kr_n) \right] \left[\vec{j}_e(r_e) \cdot \vec{A}^{i}_{LM}(kr_e) \right] , \; r_n \geq r_e .$$

The A^i_{LM} are standing wave Maxwell vector potentials in the solenoidal gauge. B^i_{LM} is identical with A^i_{LM} except that j_L is replaced by h_L so that these are outgoing waves. The i refers to either the magnetic, electric, or longitudinal mode of the field

Due to parity and angular momentum selection rules the interaction either contains the magnetic part or the electric and longitudinal parts. Since the topic of interest here is E1 conversion we consider only the electric and longitudinal parts. We define M(EL) by writing Eq. (34) in the form $N_e = 2\pi/137\left|M(EL)\right|^2$. Using Eqs. (35) and (36), M(EL) can be written in the form

$$
\begin{aligned}
(4\pi ik)^{-1}\, M(EL) = &- \int_0^\infty d\tau_n \rho_n j_L(kr_n) Y^*_{LM}(\hat{r}_n) \int_{r_n}^\infty d\tau_e \rho_e h_L(kr_e) Y_{LM}(\hat{r}_e) \\
&- \int_0^\infty d\tau_n \rho_n h_L(kr_n) Y^*_{LM}(\hat{r}_n) \int_0^{r_n} d\tau_e \rho_e j_L(kr_e) Y_{LM}(\hat{r}_e) \\
&+ \int_0^\infty d\tau_n \vec{j}_n \cdot \vec{A}^{\ell *}_{LM}(kr_n) \int_{r_n}^\infty d\tau_e \vec{j}_e \cdot \vec{B}^{\ell}_{LM}(kr_e) + \\
&+ \int_0^\infty d\tau_n \vec{j}_n \cdot \vec{B}^{\ell *}_{LM}(kr_n) \int_0^{r_n} d\tau_e \vec{j}_e \cdot \vec{A}^{\ell}_{LM}(kr_e) \\
&+ \int_0^\infty d\tau_n \vec{j}_n \cdot \vec{A}^{e *}_{LM}(kr_n) \int_{r_n}^\infty d\tau_e \vec{j}_e \cdot \vec{B}^{e}_{LM}(kr_e) \\
&+ \int_0^\infty d\tau_n \vec{j}_n \cdot \vec{B}^{e *}_{LM}(kr_n) \int_0^{r_n} d\tau_e \vec{j}_e \cdot \vec{A}^{e}_{LM}(kr_e). \qquad (37)
\end{aligned}
$$

The electric i = e and the longitudinal i = ℓ vector potentials corresponding to angular momentum L and z component M can be written in the form

$$\vec{A}^{e}_{LM}(kr) = \frac{1}{k\sqrt{L(L+1)}}\left[\vec{\nabla}\frac{d}{dr} + k^2\,\hat{r}\right] r\, j_L(kr) Y_{LM}(\hat{r}),$$

$$\vec{A}^{\ell}_{LM}(kr) = \frac{1}{k}\vec{\nabla}\, j_L(kr) Y_{LM}(\hat{r}). \tag{38}$$

By using the continuity equations

$$\vec{\nabla}\cdot\vec{j}_e + ik\rho_e = 0,$$

$$\vec{\nabla}\cdot\vec{j}_n - ik\rho_n = 0, \tag{39}$$

and performing several partial integrations it can be shown that M(EL) can be written in the form

$$\frac{\sqrt{L(L+1)}}{4\pi i} M(EL) = \int_0^\infty d\tau_n \vec{j}_n\cdot\vec{A}^{e*}_{LM}(kr_n)\int_0^\infty d\tau_e\left[\vec{j}_e\cdot k^2\hat{r}_e + \rho_e ik\frac{d}{dr_e}\right] r_e h_L(kr_e) Y_{LM}(\hat{r}_e)$$

$$+\left\{\int_0^\infty d\tau_n \vec{j}_n\cdot\vec{B}^{e*}_{LM}(kr_n)\int_0^{r_n} d\tau_e\left[\vec{j}_e\cdot k^2\hat{r}_e + \rho_e ik\frac{d}{dr_e}\right] r_e j_L(kr_e) Y_{LM}(\hat{r}_e)\right.$$

$$-\int_0^\infty d\tau_n \vec{j}_n\cdot\vec{A}^{e*}_{LM}(kr_n)\int_0^{r_n} d\tau_e\left[\vec{j}_e\cdot k^2\hat{r}_e + \rho_e ik\frac{d}{dr_e}\right] r_e h_L(kr_e) Y_{LM}(\hat{r}_e)$$

$$\left.-\frac{i}{\sqrt{L(L+1)}}\int_0^\infty d\tau_n \vec{j}_n\cdot\vec{r}_n\left[\int \vec{j}_e\cdot\vec{r}_e\, Y_{LM}\, d\Omega_e\right]_{r_e = r_n}\right\}. \tag{40}$$

The first term represents the usual conversion coefficient. The three terms in the curly brackets are penetration terms and will vanish for the case of a point nucleus. Recalling that the vector potentials contain both a gradient and a radial part we must therefore

distinguish two characteristically different penetration matrix elements.

After performing the angular integration over the electron wave function the amplitude can be written in the form

$$M_{fi}(EL) = N_{LM}\left[R_{fi}\, q_L \int_0^\infty \vec{j}_n \cdot \vec{A}^*_{LM}\,(kr_n)\,d\tau_n + \int_0^\infty d\tau_n \vec{j}_n \cdot \vec{\nabla}\,\Phi\,(r_n) Y^*_{LM}(\hat{r}_n) + \int_0^\infty d\tau_n \vec{j}_n \cdot \frac{\hat{r}_n}{r_n}\,\Theta\,(r_n) Y^*_{LM}(\hat{r}_n)\right] . \quad (41)$$

$\int_0^\infty \vec{j}_n \cdot \vec{A}^*_{LM}\,(kr_n)\,d\tau_n$ is the normal gamma-ray matrix element and R_{fi} is the radial integral over the electron initial and final wave functions, denoted by i and f. The factor q is just a constant and is given by

$$q_L = k\sqrt{\frac{L}{L+1}}\;\frac{(2L+1)!!}{(kR)^L} \quad . \quad (42)$$

Denoting the components of the Dirac electron radial wave functions by f and g, R_{fi} can be expressed in the form

$$R_{fi} = \int_0^\infty r^2 dr\; Q\; r\; h_L(kr) \quad . \quad (43)$$

The penetration weighting functions Φ and Θ are given by the relations

$$\Phi(r) = \frac{(2L+1)!!}{(kR)^L (L+1)}\left[\left(\frac{d}{dr}\, r\, h_L(kr)\right)\int_0^r r^2 dr\; Q\; r j_L(kr) - \left(\frac{d}{dr}\, r\, j_L(kr)\right)\int_0^r r^2 dr\; Q\; r h_L(kr)\right] ,$$

$$\Theta(r) = \frac{(2L+1)!!}{(kR)^L(L+1)} \left[- i(g_f f_i - f_f g_i) r^3 + (kr)^2 h_L(kr) \int_0^r r^2 dr \; Q r j_L(kr) \right.$$

$$\left. - (kr)^2 j_L(kr) \int_0^r r^2 dr \; Q \, r h_L(kr) \right] , \qquad (44)$$

where

$$Q = (g_f f_i - f_f g_i)k - (f_f f_i + g_f g_i) \frac{d}{dr} \quad . \qquad (45)$$

APPENDIX II

REDUCTION OF THE PENETRATION AND GAMMA-RAY OPERATORS

Gamma-Ray

The matrix element for gamma-ray emission is given by

$$\int \vec{j}\cdot\vec{A}^{*}_{LM}\, d\tau .$$

Using Eq. (38) given in Appendix I for A_{LM} we can write this matrix element as

$$\int \vec{j}\cdot\vec{A}^{*}_{LM}\, d\tau = \frac{1}{k\sqrt{L(L+1)}} \int \vec{j}\cdot\left[\vec{\nabla}\frac{d}{dr} + k^2\hat{r}\right] r\, j_L(kr) Y^{*}_{LM}(\hat{r}) . \tag{46}$$

Expanding $j_L(kr)$ in powers of kr gives

$$\int \vec{j}\cdot\vec{A}_{LM} d\tau = \sqrt{\frac{L+1}{L}}\ \frac{(kR)^L}{k(2L+1)!!}\left[\int \vec{j}\cdot\vec{\nabla}\left(\frac{r}{R}\right)^L Y^{*}_{LM} - (kR)^2\left\{\frac{L+3}{2(L+1)(2L+3)}\int \vec{j}\cdot\vec{\nabla}\left(\frac{r}{R}\right)^{L+2} Y^{*}_{LM} - \int \vec{j}\cdot\frac{\hat{r}}{r}\left(\frac{r}{R}\right)^{L+2} Y^{*}_{LM}\right\} + \ldots\right] . \tag{47}$$

In the long wavelength limit the higher order terms which are weighted by powers of kR are neglected and we have

$$\int \vec{j}\cdot A^{*}_{LM} d\tau = \sqrt{\frac{L+1}{L}}\ \frac{1}{(2L+1)!!}\int \vec{j}\cdot\vec{\nabla}\, r^L Y^{*}_{LM} . \tag{48}$$

Spin Current Penetration

Using the spin current $\vec{j}_s = \frac{e\mu}{2M}\vec{\nabla} \times (\psi^{*}_f \vec{\sigma}\, \psi_i)$ we can write the

penetration matrix element in the form

$$\int \vec{j}_s \cdot \frac{\hat{r}}{R}\left(\frac{r}{R}\right)^N Y_1^* \, d\tau = \frac{e\mu}{2MR^{N+1}}\left[\int \vec{\nabla}\cdot\left[(\psi_f^* \vec{\sigma} \psi_i) \times \hat{r}\, r^N Y_1^*\right] d\tau\right.$$

$$\left. + \int (\psi_f^* \vec{\sigma} \psi_i)\cdot\vec{\nabla} \times (\hat{r}\, r^N Y_1^*) d\tau\right] . \qquad (49)$$

The first term can be transformed to a vanishing surface integral and the second term can be rewritten in the form

$$\int \vec{j}_s \cdot \frac{\hat{r}}{R}\left(\frac{r}{R}\right)^N Y_1^* \, d\tau = \frac{e\mu}{2MR^{N+1}} \int (\psi_f^* \vec{\sigma} \psi_i)\cdot\left[\vec{\nabla}\,(r^{N-1}Y_1^*) \times \vec{r}\right] d\tau. \qquad (50)$$

Using $\vec{L} = -\vec{r} \times i\vec{\nabla}$ we finally have

$$\int j_s \cdot \frac{\hat{r}}{R}\left(\frac{r}{R}\right)^N Y_1^* d\tau = \frac{e\mu}{i2MR^{N+1}} \int \psi_f^* \vec{\sigma}\cdot\vec{L}\,(r^{N-1}Y_1^*)\psi_i d\tau. \qquad (51)$$

Convection Current Penetration

Using the convection current $\vec{j}_c = \frac{e}{2iM}[\psi_f^* \vec{\nabla} \psi_i - \psi_i \vec{\nabla} \psi_f^*]$ we can write the penetration matrix element in the form

$$\int j_c \cdot \frac{\hat{r}}{R}\left(\frac{r}{R}\right)^N Y_1^* \, d\tau = -\frac{e}{2iMR^{N+1}}\left[\int \vec{\nabla}(\psi_f^*\psi_i)\cdot\hat{r}\, r^N Y_1^* d\tau - 2\int \psi_f^* \vec{\nabla}\psi_i \cdot \hat{r}\, r^N Y_1^* d\tau\right] . \qquad (52)$$

Using standard vector identities the first of these terms can be written as

$$\int \vec{\nabla}(\psi_f^*\psi_i)\cdot\hat{r}\, r^N Y_1^* d\tau = \int \vec{\nabla}\cdot(\hat{r}\, r^N Y_1^* \psi_f^* \psi_i) d\tau - \int (\vec{\nabla}\cdot\vec{r}) r^{N-1} Y_1^* \psi_f^* \psi_i d\tau$$

$$- \int \psi_f^* \psi_i \, \vec{r}\cdot\vec{\nabla}\,(r^{N-1}Y_1^*) d\tau . \qquad (53)$$

The first of these three terms can be transformed to a vanishing surface integral and the other two terms can be combined to give

$$\int \vec{\nabla} (\psi_f^* \psi_i) \cdot \hat{r}\, r^N Y_l^* d\tau = -(N+2) \int r^{N-1} Y_l^* \psi_f^* \psi_i d\tau \ . \qquad (54)$$

Therefore the penetration matrix element can be written in the form

$$\int \vec{j}_c \cdot \frac{\hat{r}}{R} \left(\frac{r}{R}\right)^N Y_l^* \, d\tau = \frac{e}{iMR^{N+1}} \int \psi_f^* \, r^{N-1} Y_l^* \left(\vec{r} \cdot \vec{\nabla} + \frac{N+2}{2}\right) \psi_i d\tau \ . \qquad (55)$$

APPENDIX III

FORM OF THE ATOMIC WEIGHTING COEFFICIENTS

To obtain the form of the weighting coefficients, the penetration weighting functions Φ and Θ presented in Appendix I must be evaluated in terms of the initial and final electron wave functions. These weighting functions for L = 1 are

$$\Phi(r) = \frac{3}{2kR}\left[\left(\frac{d}{dr}\, rh_1(kr)\right)\int_0^r r^2 drQrj_1(kr) - \left(\frac{d}{dr}\, rj_1(kr)\right)\int_0^r r^2 drQrh_1(kr)\right] ,$$

$$\Theta(r) = \frac{3}{2kR}\left[-i(g_f f_i - f_f g_i)r^3 + (kr)^2 j_1(kr)\int_0^r r^2 drQrj_1(kr) - (kr)^2 j_1(kr)\right.$$

$$\left.\int_0^r r^2 drQrh_1(kr)\right] ,$$

where

$$Q = (g_f f_i - f_f g_i)k - (f_f f_i + g_f g_i)\frac{d}{dr} .$$

We will represent the functions Θ and Φ in the form of a power series in r/R and determine the form of the coefficients of the two lowest order terms. Since the electron radial functions f and g are only needed for small r these functions are expanded in a power series about r = 0:

$$\kappa < 0: \qquad rg(r) = \left(\frac{r}{R}\right)^{|\kappa|}\sum_{n=0}^{\infty} a_n\left(\frac{r}{R}\right)^{2n} ,$$

$$rf(r) = \left(\frac{r}{R}\right)^{|\kappa|+1}\sum_{n=0}^{\infty} b_n\left(\frac{r}{R}\right)^{2n} ,$$

$$\kappa > 0: \qquad rg(r) = \left(\frac{r}{R}\right)^{\kappa+1} \sum_{n=0}^{\infty} a_n \left(\frac{r}{R}\right)^{2n} ,$$

$$rf(r) = \left(\frac{r}{R}\right)^{\kappa} \sum_{n=0}^{\infty} b_n \left(\frac{r}{R}\right)^{2n} , \tag{56}$$

where κ is the usual relativistic quantum number and the constants a_n and b_n are determined numerically by solution of the Dirac equation. We also represent the spherical Bessel and Hankel functions in the long wavelength limit,

$$j_1(kr) = \frac{kr}{3} , \quad h_1(kr) = - \frac{i}{(kr)^2} . \tag{57}$$

We first consider the case $\kappa_i = -1$, $\kappa_f = +1$. For this case keeping only the two lowest order terms, the wave functions are

$$\begin{aligned} rg_i &= a_0^i \left(\frac{r}{R}\right) + a_1^i \left(\frac{r}{R}\right)^3 , \\ rf_i &= b_0^i \left(\frac{r}{R}\right)^2 + b_1^i \left(\frac{r}{R}\right)^4 , \\ rg_f &= a_0^f \left(\frac{r}{R}\right)^2 + a_1^f \left(\frac{r}{R}\right)^4 , \\ rf_f &= b_0^f \left(\frac{r}{R}\right) + b_1^f \left(\frac{r}{R}\right)^3 . \end{aligned} \tag{58}$$

We define new quantities in terms of the wave function coefficients

$$A_1 = a_0^i \, b_0^f , \quad A_2 = a_1^i \, b_0^f + a_0^i \, b_1^f ,$$

$$B_1 = b_0^i \, a_0^f , \quad B_2 = b_0^i \, a_1^f + b_1^i \, a_0^f ,$$

$$C_1 = b_0^i\, b_0^f \ , \quad C_2 = b_1^i\, b_0^f + b_0^i\, b_1^f \ ,$$

$$D_1 = a_0^i\, a_0^f \ , \quad D_2 = a_1^i\, a_0^f + a_0^i\, a_1^f \ .$$

The subscript 1 denotes products of first order wave function coefficients and the subscript 2 denotes products of first and second order wave function coefficients.

The operator r^2Q can now be expressed as

$$r^2Q = \left[- A_1\left(\frac{r}{R}\right)^2 + (B_1 - A_2)\left(\frac{r}{R}\right)^4 \right] k - \left[(C_1 + D_1)\left(\frac{r}{R}\right)^3 + (C_2 + D_2)\left(\frac{r}{R}\right)^5 \right] \frac{d}{dr} \ . \quad (60)$$

Substituting this into the expressions for Φ and Θ gives

$$\Phi = \frac{i}{k}\left[- \frac{3}{5} A_1 + \frac{3}{10} \frac{C_1 + D_1}{kR} \right]\left(\frac{r}{R}\right)^3 + \frac{i}{k}\left[\frac{-21A_2 - 27B_1}{140} - \frac{C_1 + D_1}{30} kr + \frac{3}{28} \frac{C_2 + D_2}{kR} \right]\left(\frac{r}{R}\right)^5$$

$$\Theta = \frac{i}{k} \frac{3A_1}{2} \left(\frac{r}{R}\right)^3 + \frac{i}{k}\left[\frac{3A_2 + 6B_1}{5} + \frac{C_1 + D_1}{30} kR \right]\left(\frac{r}{R}\right)^5 \ . \quad (61)$$

We define the weighting coefficients γ_1, γ_2, β_1, and β_2 by the relations

$$\Phi = \gamma_1 \left(\frac{r}{R}\right)^3 + \gamma_2 \left(\frac{r}{R}\right)^5$$

$$\Theta = \beta_1 \left(\frac{r}{R}\right)^3 + \beta_2 \left(\frac{r}{R}\right)^5 \ . \quad (4)$$

We present in Table XIV below the values of these coefficients for the transitions required for E1 conversion.

TABLE XIV

FORM OF THE ATOMIC WEIGHTING COEFFICIENTS

κ_i, κ_f	$\frac{k}{i}\gamma_1$	$\frac{k}{i}\gamma_2$	$\frac{k}{i}\beta_1$	$\frac{k}{i}\beta_2$
-1, +1	$\frac{-3A_1}{2} + \frac{3(C_1 + D_1)}{10kR}$	$\frac{-21A_2 - 27B_1}{140} - \frac{(C_1 + D_1)kR}{30} + \frac{3(C_2 + D_2)}{28kR}$	$\frac{3A_1}{2}$	$\frac{3A_2 + 6B_1}{5} + \frac{(C_1 + D_1)kR}{30}$
-1, -2	$\frac{3D_1}{10kR}$	$\frac{-D_1kR}{30} + \frac{3(C_1 + D_2)}{28kR} + \frac{15A_1 + 9B_1}{140}$	0	$\frac{D_1kR}{30} + \frac{-15A_1 - 3B_1}{20}$
+1, -1	$\frac{3B_1}{5} + \frac{3(C_1 + D_1)}{10kR}$	$\frac{27A_1 + 21B_2}{140} - \frac{(C_1 + D_1)kR}{30} + \frac{3(C_2 + D_2)}{28kR}$	$\frac{-3B_1}{2}$	$\frac{-6A_1 - 3B_2}{5} + \frac{(C_1 + D_1)kR}{30}$
+1, +2	$\frac{3C_1}{10kR}$	$\frac{-C_1kR}{30} + \frac{3(C_2 + D_1)}{28kR} - \frac{9A_1 + 15B_1}{140}$	0	$\frac{C_1kR}{30} + \frac{3A_1 + 15B_1}{20}$
-2, +1	$\frac{3D_1}{10kR}$	$\frac{-D_1kR}{30} + \frac{3(C_1 + D_2)}{28kR} - \frac{9A_1 + 15B_1}{140}$	0	$\frac{D_1kR}{30} + \frac{3A_1 + 15B_1}{20}$

REFERENCES

1. M.E. Rose, Internal Conversion Coefficients (North Holland Pub. Co., Amsterdam, 1958).

2. L.A. Sliv and I.M. Band, Coefficients of Internal Conversion of Gamma Radiation, Part I - K Shell (Physico-Technical Institute Academy of Science, Leningrad, U.S.S.R., 1956; issued in U.S. as Report 571CC K1, Physics Dept., University of Illinois, Urbana, Ill.).

   L.A. Sliv and I.M. Band, Coefficients of Internal Conversion of Gamma Radiation, Part II - L Shell (Physico-Technical Institute Academy of Science, Leningrad, U.S.S.R., 1958; issued in U.S. as Report 581CC L1, Physics Dept., University of Illinois, Urbana, Ill.).

3. L.A. Sliv, Zhur. Eksptl. Teoret. Fiz. 21, 770 (1951).

4. E.L. Church and J. Weneser, Phys. Rev. 104, 1382 (1956).

5. F. Asaro, F.S. Stephans, J.M. Hollander and I. Perlman, Phys. Rev. 117, 492 (1960).

6. A.H. Wapstra and G.J. Nijgh, Nuclear Phys. 1, 245 (1956).

7. Z. Grabowski, B.G. Pettersson, T.R. Gerholm and J.E. Thun, Nuclear Phys. 24, 251 (1961).

8. E.S. Snyder and S. Frankel, Phys. Rev. 106, 755 (1957).

9. C.J. Herrlander and R.L. Graham, Nuclear Phys. 58, 544 (1964).

10. T.R. Gerholm, B.-G. Pettersson, B. van Nooijen and Z. Grabowski, Nuclear Phys. 24, 177 (1961).

11. C.J. Herrlander and G.T. Ewan, Proceedings of the International Conference of Atomic Electrons in Nuclear Transformations (The Office of Scientific, Technical, and Economical Information, Warsaw, Poland, 1963).

12. T.R. Gerholm, B.-G Pettersson, and Z. Grabowski, Nuclear Phys. 65, 441 (1965).

13. G. Kramer, Zeit. Physik 146, 187 (1956); 147, 628 (1957).

14. G. Kramer and S.G. Nilsson, Nuclear Phys. 35, 273 (1962).

15. T.A. Green and M.E. Rose, Phys. Rev. 110, 105 (1958).

16. S.G. Nilsson and J.O. Rasmussen, Nuclear Phys. 5, 617 (1958).

17. E.L. Church and J. Weneser, Ann. Rev. Nuclear Sci. 10, 193 (1960).

18. J.M. Blatt and V.F. Weisskopf, Theoretical Nuclear Physics (John Wiley and Sons, Inc., New York, N.Y., 1952) p. 627.

19. O. Nathan and S.G. Nilsson "Collective Nuclear Motion and the Unified Model", Alpha-, Beta- and Gamma-Ray Spectroscopy (North Holland Publishing Co., Amsterdam, 1965) Vol. 2 p. 601.

20. A.K. Kerman "Nuclear Rotational Motion", Nuclear Reactions (North Holland Pub. Co., Amsterdam, 1959) Vol. 1, p. 429.

21. J.P. Elliot, Collective Motion in Nuclei (Univ. of Rochester Report NYO-2271, Rochester, N.Y., 1958).

22. S.G. Nilsson, Kgl. Danske Videnskab. Selskab Mat.-fys. Medd. 29, No. 16 (1955).

23. G. Alaga, Phys. Rev. 100, 432 (1955).

24. E.L. Church and J. Weneser, Nuclear Phys. 28, 602 (1961).

25. U. Hauser, K. Runge and G. Knissel, Nuclear Phys. 27, 632 (1961).

26. P. Alexander, F. Boehm and E. Kankeleit, Phys. Rev. 133, B284 (1964).

27. Nuclear Data Sheets, National Academy of Sciences, National Research Council (1960).

28. P. Alexander and F. Boehm, Nuclear Phys. 46, 108 (1962).

29. B. Harmatz and T.H. Handley, Phys. Rev. 128, 1186 (1962).

30. W.F. Edwards, F. Boehm, J. Rogers and E.J. Seppi, Nuclear Phys. 63, 97 (1965).

31. P. Alexander and R.S. Hager, Phys. Rev. 139, B288 (1965).

32. P. Alexander, J.W.M. DuMond and H.E. Henrikson, Design and Construction of a 35 cm Radius $\sqrt{2}\,\pi$ Iron-Free Beta Spectrometer unpublished California Institute of Technology Report (1964).

33. W.M. Gibson, G.L. Miller and P.F. Donovan "Semiconductor Particle Spectrometers", Alpha-, Beta- and Gamma-Ray Spectroscopy (North Holland Pub. Co., Amsterdam, 1965), Vol. 2, p. 345.

34. C.P.O. Günther, Private communication.

35. E. Kankeleit, Rev. Sci. Instr. 35, 194 (1965).

36. E.J. Callan, Proceedings of the International Conference of Atomic Electrons in Nuclear Transformations (The Office of Scientific, Technical, and Economical Information, Warsaw, Poland, 1963).

37. E. Seltzer and R. Hager, Physics Letters 18, 163 (1965).

38. E. Seltzer, Ph.D. Thesis, California Institute of Technology,1965.

39. A. Bohr and B.R. Mottelson, Kgl. Danske Videnskab. Selskab Mat.-fys. Medd. 27, No. 16 (1953).

40. A.J. Rassey, Phys. Rev. 109, 949 (1957).

41. E. Bodenstedt and J.D. Rogers "Magnetic Moments of Excited Nucleon States", Perturbed Angular Correlations (North Holland Pub. Co., Amsterdam, 1964) p. 91.

42. L. Chiao and J.O. Rasmussen, Proceedings of the International Conference of Nuclear Structure, Kingston, Canada (Univ. of Toronto Press, Toronto, 1961) p. 646.

43. S.T. Belyaev, Kgl. Danske Videnskab. Selskab Mat.-fys. Medd. 31, No. 11 (1959).

44. Yu.T. Grin, Soviet Physics JETP, 12, 100 (1961).

45. G. Monsonego and R. Piepenbring, Nuclear Phys. 58, 593 (1964).

46. N.I. Pyatov, Acta Phys. Polon. 25, 21 (1964).

47. M.N. Vergnes and J.O. Rasmussen, Nuclear Phys. 62, 233 (1965).

48. H. Frauenfelder and R.M. Steffen, "Angular Correlations", Alpha-Beta- and Gamma-Ray Spectroscopy (North Holland Pub. Co., Amsterdam, 1965) Vol. 1, p. 997.

49. J.E. Thun, Z. Grabowski, M.S. El-Nesr and G. Bruce, Nuclear Phys. 29, 1 (1962).

50. L.C. Biedenharn and M.E. Rose, Rev. Mod. Phys. 25, 729 (1953).

51. A.K. Kerman, Kgl. Danske Videnskab. Selskab Mat.-fys. Medd. 30, No. 15 (1956).

52. C.J. Gallagher and V.G. Soloviev, Mat. Fys. Skr. Dan. Vid. Selsk. 2, No. 2 (1962).

53. D.R. Bes, P. Federman, E. Maqueda and A. Zuker, Nuclear Phys. 65, 1 (1965).

54. M. Baranger, Phys. Rev. 120, 957 (1960).

55. M.E. Rose, Multipole Fields (John Wiley and Sons, Inc., 1955).